

Big-Bang Nucleosynthesis Reactions Catalyzed by a Long-Lived Negatively Charged Leptonic Particle

Masayasu KAMIMURA,^{1,3} Yasushi KINO² and Emiko HIYAMA³

¹*Department of Physics, Kyushu University, Fukuoka 812-8581, Japan*

²*Department of Chemistry, Tohoku University, Sendai 980-8578, Japan*

³*RIKEN Nishina Center, RIKEN, Wako 351-0198, Japan*

An accurate quantum three-body calculation is performed for the new type of big-bang nucleosynthesis (BBN) reactions that are catalyzed by a hypothetical long-lived negatively charged, massive leptonic particle (called X^-) such as the supersymmetric (SUSY) particle *stau*, the scalar partner of the tau lepton. It is known that if the X^- particle has a lifetime of $\tau_X \gtrsim 10^3$ s, it can capture a light element previously synthesized in standard BBN and form a Coulombic bound state, for example, (${}^7\text{Be}X^-$) at temperature $T_9 \lesssim 0.4$ (in units of 10^9 K), (αX^-) at $T_9 \lesssim 0.1$ and (pX^-) at $T_9 \lesssim 0.01$. The bound state, an exotic atom, is expected to induce the following reactions in which X^- acts as a catalyst: i) α -transfer reactions such as (αX^-) + $d \rightarrow {}^6\text{Li} + X$, ii) radiative capture reactions such as (${}^7\text{Be}X^-$) + $p \rightarrow ({}^8\text{B}X^-) + \gamma$, iii) three-body breakup reactions such as (${}^7\text{Li}X^-$) + $p \rightarrow \alpha + \alpha + X^-$, iv) charge-exchange reactions such as (pX^-) + $\alpha \rightarrow (\alpha X^-) + p$ and v) neutron induced reactions such as (${}^8\text{Be}X^-$) + $n \rightarrow {}^9\text{Be} + X^-$. In recent papers it has been claimed that some of these X^- -catalyzed reactions have significantly large cross sections so that the inclusion of the reactions into the BBN network calculation can markedly change the abundances of some elements, giving not only a solution to the ${}^6\text{Li}$ - ${}^7\text{Li}$ problem (the calculated underproduction of ${}^6\text{Li}$ by a factor of ~ 1000 and overproduction of ${}^7\text{Li}$ + ${}^7\text{Be}$ by a factor of ~ 3) but also a constraint on the lifetime and primordial abundance of the elementary particle X^- . However, most of these calculations of the reaction cross sections in the literature were performed assuming too naive models or approximations that are unsuitable for these complicated low-energy nuclear reactions. We use a high-accuracy few-body calculation method developed by the authors and provide precise cross sections and rates of these catalyzed BBN reactions for use in the BBN network calculation.

§1. Introduction

The accurate theoretical prediction of nuclear reaction rates is of essential importance in the study of big-bang nucleosynthesis (BBN) when particular reaction rates are very difficult or even impossible to estimate experimentally. The most typical example of such reactions is the production and destruction of light elements catalyzed by a hypothetical long-lived negatively charged massive ($\gtrsim 100$ GeV) leptonic particle, here denoted as X^- ; a candidate for this particle is the supersymmetric (SUSY) counterpart of the tau lepton (τ), i.e., the stau ($\tilde{\tau}$).^{*} Recently, BBN involving these X^- -catalyzed nuclear reactions has been extensively studied from the viewpoint of particle-physics catalysis in BBN,^{1)–14)} which may be briefly reviewed as follows (and precisely reviewed in Refs. 12) and 14) and references therein):

i) If the X^- particle has a lifetime on the order of 10^3 s or longer, it can capture a light nucleus, A , previously synthesized during BBN, and produce a bound state

^{*}) The stau is one of the particles expected to be discovered at the CERN Large Hadron Collider.¹⁵⁾

denoted as (AX^-) , which is a type of exotic atom with the nucleus A in a Coulombic orbit around the massive X^- at the center.*)

ii) When the cosmic temperature cools to $T_9 \sim 0.4$ (in units of 10^9 K) after the standard BBN ($T_9 \gtrsim 0.5$), X^- captures ${}^7\text{Be}$ to form $({}^7\text{Be}X^-)$, which is subsequently destroyed by the $({}^7\text{Be}X^-) + p \rightarrow ({}^8\text{B}X^-) + \gamma$ reaction⁶⁾ followed by the β -decay of $({}^8\text{B}X^-)$ to $\alpha + \alpha + X^-$.

iii) At $T_9 \sim 0.3$, X^- captures ${}^7\text{Li}$ to generate $({}^7\text{Li}X^-)$, which is subsequently destroyed by the $({}^7\text{Li}X^-) + p \rightarrow \alpha + \alpha + X^-$ reaction.

iv) At $T_9 \sim 0.1$, X^- particles capture α particles to form (αX^-) in abundance which triggers the reaction $(\alpha X^-) + d \rightarrow {}^6\text{Li} + X^-$ to produce an enormous amount of ${}^6\text{Li}$, as originally proposed by Pospelov¹⁾ and confirmed by Hamaguchi *et al.*⁵⁾ including two of the present authors (M. K. and Y. K.).

v) At $T_9 \sim 0.01$, although X^- particles start capturing protons to form (pX^-) , its abundance remains low due to the charge-exchange reaction $(pX^-) + \alpha \rightarrow (\alpha X^-) + p$, which occurs before (pX^-) begins to interact with other nuclei to form heavier elements.¹⁴⁾

The contribution of these reactions is expected to modify standard BBN (SBBN in short) and to solve the calculated underproduction (by a factor of ~ 1000) of the primordial abundance of ${}^6\text{Li}$ and the overproduction (by a factor of ~ 3) of ${}^7\text{Li}$,¹⁶⁾ and, at the same time, to provide information for constraining the lifetime and primordial abundance of the elementary particle X^- . However, full quantum mechanical studies of the reactions have not been performed on the basis of nuclear reaction theory except for the work of Ref. 5) on the production of ${}^6\text{Li}$.

The purpose of the present paper is to perform a precise quantum three-body calculation of the cross sections of many types of catalyzed BBN (CBBN in short) reactions including those mentioned above in i) – v) and to provide their reaction rates for use in the BBN network calculation. The adopted theoretical method and numerical technique have been developed by the present authors, reviewed in Ref. 17), and are well established in the field of few-body atomic and nuclear systems.

The CBBN reactions studied in this paper are classified into four types:

1) *Transfer reactions:*

$$(AX^-) + a \rightarrow B + X^-, \quad (1-1)$$

where A is picked up by an incoming nucleus a to produce a nucleus $B(= A + a)$,

2) *Radiative capture reactions:*

$$(AX^-) + a \rightarrow (BX^-) + \gamma, \quad (1-2)$$

3) *Three-body breakup reactions:*

$$(AX^-) + a \rightarrow b_1 + b_2 + X^-, \quad (1-3)$$

4) *Charge-exchange reactions:*

$$(AX^-) + a \rightarrow (aX^-) + A. \quad (1-4)$$

*) For instance, the binding energies of $({}^7\text{Be}X^-)$ and (αX^-) are ~ 1.3 and ~ 0.34 MeV, and the rms radii are ~ 3.6 and ~ 7 fm, respectively.

We solve the Schrödinger equations of CBBN reactions (1.1)–(1.4), explicitly taking the three-body degree of freedom into account, and derive their cross sections and reaction rates at incoming energies below 200 keV.

Throughout this paper, it is not necessary to identify X^- with any particular particle such as the SUSY particle stau, although this is assumed, for instance, in Refs. 4), 5) and 14). The property of X^- we assume here is that it has a charge of $-e$, a mass $m_X \gtrsim 100$ GeV and a lifetime $\tau_X \gtrsim 10^3$ s and that it interacts with light elements via the Coulomb force only.

The structure of the present paper is as follows. We investigate X^- -catalyzed α -transfer reactions that produce ${}^6\text{Li}$, ${}^7\text{Li}$ and ${}^7\text{Be}$ in §2, resonant and nonresonant radiative capture reactions that destroy ${}^7\text{Be}$ in §3, three-body breakup reactions that destroy ${}^6\text{Li}$ and ${}^7\text{Li}$ in §4, the charge-exchange reactions in §5 and the possibility of the X^- -catalyzed primordial production of ${}^9\text{Be}$ in §6. A summary is given in §7.

§2. X^- -catalyzed α -transfer reactions

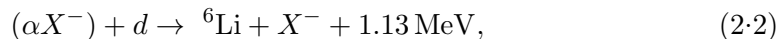
2.1. Necessity of three-body calculation

2.1.1. Production of ${}^6\text{Li}$

One of the puzzles in SBBN is that the BBN prediction of the ${}^6\text{Li}$ abundance is a factor of ~ 1000 smaller than the observed data.¹⁶⁾ The too small prediction is mostly because the radiative capture reaction that produces ${}^6\text{Li}$ in SBBN,



is heavily E1-hindered with a very small astrophysical S -factor, $S_\gamma \sim 2 \times 10^{-6}$ keV b.¹⁸⁾ To obtain a much greater production of ${}^6\text{Li}$, Pospelov considered,¹⁾ for the first time, a new type of CBBN reaction,



in which the bound state^{*)} (αX^-) promotes the synthesis of α and d to form ${}^6\text{Li}$ with no photon emission. He claimed that the S -factor of the X^- -catalyzed reaction (2.2), say S_X , is enhanced by 8 orders of magnitude ($S_X \sim 3 \times 10^2$ keV b) compared with S_γ and that the abundance of ${}^6\text{Li}$ is greatly increased so that the ${}^6\text{Li}$ problem can be solved under a suitable restriction on the abundance and lifetime of X^- .

His estimation of S_X , however, was based on a too naive comparison between (2.1) and (2.2). Namely, in an analogy to the real photon in (2.1) with the wavelength $\lambda_\gamma \sim 130$ fm, Pospelov introduced a virtual photon in (2.2) with a characteristic wavelength λ_X on the order of the Bohr radius ($= 3.63$ fm) of the atom (αX^-) and assumed the scaling relation^{**)}

$$\frac{S_X}{S_\gamma} \sim \left(\frac{\lambda_\gamma}{\lambda_X} \right)^{2\ell+1}, \quad (2.3)$$

*) Hereafter, when (AX^-) is in the $1s$ ground state, the suffix $1s$ of $(AX^-)_{1s}$ is omitted.

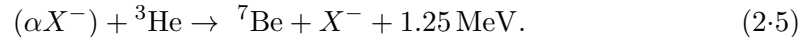
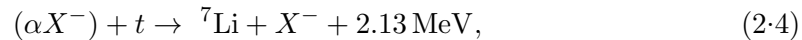
***) A more detailed expression is given by Eq. (4) in Ref. 1) but the scaling relation is essentially described by (2.3).

where the photon multipolarity ℓ is assumed to be $\ell = 2$ (namely, E2), not only for the real photon^{*)} but also for the virtual one. In this case, the enhancement ratio S_X/S_γ amounts to $\sim 10^8$.

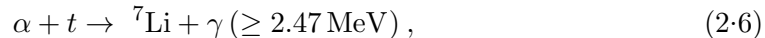
However, the scaling relation (2.3), which compares the wavelengths of the real and virtual photons, is not suitable for discussing reaction (2.2) because the relation does not take into account the nuclear interaction, which is the most important factor in the process of transferring the α particle from (αX^-) to the deuteron to form ${}^6\text{Li}$. Therefore, two of the authors (M. K. and Y. K.) and their colleagues⁵⁾ performed a fully quantum three-body calculation of the $\alpha + d + X^-$ system and calculated the S -factor of reaction (2.2), $S_X(E)$, as a function of the incident energy E at $E = 10 - 120$ keV. The calculated S -factor at the Gamow peak energy is 38 keV b ($S_X/S_\gamma \sim 10^7$, nearly one order of magnitude smaller than that in Ref. 1)). Note that S_X of the CBBN reaction (2.2) is of a similar order of magnitude to the S -factors of nonresonant photonless SBBN reactions caused by the nuclear interaction; for example, compare S_X with the observed values of ~ 60 keV b for $d+d \rightarrow t+p$ and $\sim 5 \times 10^{-6}$ keV b for the E1-forbidden process $d+d \rightarrow \alpha+\gamma$. The large enhancement of the CBBN/SBBN ratio ($\sim 10^7$) is simply because the SBBN reaction (2.1) is heavily E1-hindered.

2.1.2. Production of ${}^7\text{Li}$ and ${}^7\text{Be}$

In the BBN network calculation with the CMB-based baryon-to-photon ratio ($\eta_B = 6.0 \times 10^{-10}$),¹⁹⁾ the abundance of ${}^7\text{Be}$ is approximately one order of magnitude larger than that of ${}^7\text{Li}$. Since ${}^7\text{Be}$ eventually decays to ${}^7\text{Li}$ by electron capture, the sum of the abundances of both ${}^7\text{Li}$ and ${}^7\text{Be}$ is regarded as the abundance of ${}^7\text{Li}$ in the ${}^7\text{Li}$ -overproduction problem. To examine the effect of CBBN on the abundance of ${}^7\text{Li}+{}^7\text{Be}$, Cyburt *et al.*⁴⁾ studied the α -transfer reactions



which produce ${}^7\text{Li}$ and ${}^7\text{Be}$ at $T_9 \sim 0.1$. Using the scaling relation proposed in Ref. 1), they claimed that the S -factors of the above CBBN reactions are 5 orders of magnitude greater than those of the E1 radiative capture reactions



which are the most effective source for producing ${}^7\text{Li}$ and ${}^7\text{Be}$ in SBBN.

However, it is clear that the enhancement ratio CBBN/SBBN in S -factors will be only on the order of $10^1 - 10^2$ contrary to the case of ${}^6\text{Li}$ production ($\sim 10^7$). The reason for this is as follows: the SBBN S -factors of (2.6) and (2.7) at astrophysical

^{*)} This assumption of $\ell = 2$ for the real photon in (2.1) may not be justified *at astrophysical energies* (no experimental data there). According to the so far most precise six-body calculation²⁰⁾ of the E1-hindered radiative capture reaction (2.1), the S -factor of the E2 transition decreases much more rapidly than that of the E1 transition as the energy decreases, and eventually the E1/E2 ratio becomes ~ 10 at $E \sim 0$ (see Figs. 7 and 8 in Ref. 20)).

energies are respectively ~ 0.1 and ~ 0.5 keV b,¹⁸⁾ which are 5 orders of magnitude larger than that of the E1-hindered reaction (2.1). Moreover, the CBBN S -factors of (2.4) and (2.5) should be significantly reduced compared with that of (2.2), because a rearrangement of the angular momenta among the three particles is needed when going from the entrance channel to the exit channel; note that a significant difference between (2.2) and (2.4)–(2.5) is that the relative motion between d and α in ${}^6\text{Li}$ is that of s -wave whereas that between $t({}^3\text{He})$ and α in ${}^7\text{Li}$ (${}^7\text{Be}$) is that of p -wave. This consideration of the CBBN/SBBN ratio will be confirmed by the quantum three-body calculation of reactions (2.4) and (2.5) in this section.

2.2. Three-body Schrödinger equation and reaction rate

Following Refs. 5) and 17), we briefly explain the three-body calculation method used to investigate the above X^- -catalyzed transfer reactions. We emphasize that the method described here is an exact method for calculating the cross section of the low-energy transfer reactions within the three-body model of the total system concerned. The present authors have previously performed the same types of calculations in the study of muon transfer reactions^{17),21)–23)} in muon-catalyzed fusion cycles.²⁴⁾

As shown in Fig. 1, we consider all three sets of the Jacobi coordinates $(\mathbf{r}_c, \mathbf{R}_c)$, $c = 1, 2$ and 3 , to completely treat the three-body degrees of freedom of the system $A + a + X^-$. Here, we take $A = \alpha$, and $a = d, t$ and ${}^3\text{He}$ for reactions (2.2), (2.4) and (2.5), respectively.

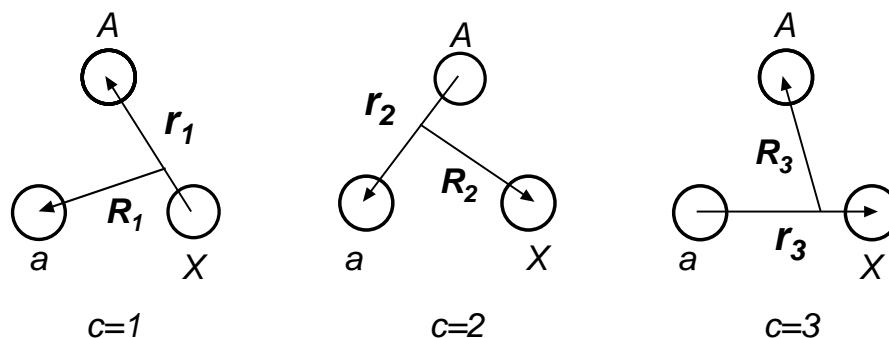


Fig. 1. Three sets of Jacobi coordinates in the $A+a+X^-$ system. The entrance channel $(AX^-)+a$ is described using the coordinate system $c = 1$, and the transfer channels $(Aa)+X^-$ and $(aX^-)+A$ are described using $c = 2$ and $c = 3$, respectively.

The Schrödinger equation for the total wave function with total energy E_{tot} , angular momentum J and z -component M is given by

$$(H - E_{\text{tot}})\Psi_{JM} = 0 \quad (2.8)$$

with the Hamiltonian

$$H = -\frac{\hbar^2}{2m_c}\nabla_{\mathbf{r}_c}^2 - \frac{\hbar^2}{2M_c}\nabla_{\mathbf{R}_c}^2 + V_{A-X}(r_1) + V_{A-a}(r_2) + V_{a-X}(r_3). \quad (2.9)$$

As far as we use the reduced masses (m_c and M_c) associated with the coordinates (\mathbf{r}_c and \mathbf{R}_c), every choice of c in the kinetic term is equivalent. The notation of the potentials is self-evident; an explicit form will be given below. The Schrödinger equation is solved under the scattering boundary condition imposed appropriately on the relevant reaction.

For all the CBBN reactions studied in this paper, only the resonant radiative capture reaction (1.2) requires serious consideration of the intrinsic spins of the particles as will be discussed in §3. In this section, for the nonresonant α -transfer reactions, the spin of the incoming particle a ($= d, t, {}^3\text{He}$) is neglected. Therefore, in the exit channel of (2.4) and (2.5), the $3/2^-$ (p -wave) ground state and the $1/2^-$ (p -wave) first excited state of ${}^7\text{Li}$ and ${}^7\text{Be}$ are degenerated energetically to their weighted mean. The validity of this approximation will be discussed in §2.6.

Firstly, we construct the wave function of the $1s$ ground state of (AX^-) in the entrance channel on the coordinate system $c = 1$ and that of the ground state of the nucleus B on $c = 2$. We denote the wave function by $\phi_{l_c m_c}^{(c)}(\mathbf{r}_c)$ and the eigenenergy by $\varepsilon_{l_c}^{(c)}$; explicitly, $l_1 = 0$ for (αX^-) , $l_2 = 0$ for ${}^6\text{Li}$ and $l_2 = 1$ for ${}^7\text{Li}$ (${}^7\text{Be}$). These quantities are obtained by solving

$$\left[-\frac{\hbar^2}{2m_c} \nabla_{\mathbf{r}_c}^2 + V_c(r_c) - \varepsilon_{l_c}^{(c)} \right] \phi_{l_c m_c}^{(c)}(\mathbf{r}_c) = 0, \quad (c = 1, 2) \quad (2.10)$$

where the potential V_c denotes V_{A-X} and V_{A-a} for $c = 1$ and 2 , respectively.

Using $\chi_{L_c M_c}^{(c)}(\mathbf{R}_c) \equiv \chi_{L_c}^{(c)}(R_c) Y_{L_c M_c}(\hat{\mathbf{R}}_c)$, we denote the scattering wave function along the coordinate \mathbf{R}_c with angular momentum L_c and z -component M_c ($c = 1, 2$). The center-of-mass (cm) scattering energy associated with the coordinate \mathbf{R}_c , say E_c , is introduced as

$$E_c = E_{\text{tot}} - \varepsilon_{l_c}^{(c)} = \hbar^2 k_c^2 / 2M_c, \quad (c = 1, 2) \quad (2.11)$$

together with the corresponding wave number k_c .

The total three-body wave function Ψ_{JM} , which describes the transfer reaction (2.2) in the most sophisticated manner, is written as^{17),25)}

$$\Psi_{JM} = \phi_{00}^{(1)}(\mathbf{r}_1) \chi_{JM}^{(1)}(\mathbf{R}_1) + \left[\phi_{l_2}^{(2)}(\mathbf{r}_2) \otimes \chi_{L_2}^{(2)}(\mathbf{R}_2) \right]_{JM} + \Psi_{JM}^{(\text{closed})}. \quad (2.12)$$

Here, the first and second terms represent the two open channels, $(AX^-) + a$ on $c = 1$ and $B + X^-$ on $c = 2$, respectively; there are no other open channels in the energy range ($E_1 < 150$ keV) that we are interested in. In the first term, the radial part $\chi_J^{(1)}(R_1)$ has incoming and outgoing amplitudes, and $\chi_{L_2}^{(2)}(R_2)$ in the second term has the outgoing amplitude only. These should satisfy the boundary condition

$$\lim_{R_c \rightarrow \infty} R_c \chi_{L_c}^{(c)}(R_c) = u_{L_c}^{(-)}(k_c, R_c) \delta_{c1} - \sqrt{\frac{v_1}{v_c}} S_{1 \rightarrow c}^{L_c} u_{L_c}^{(+)}(k_c, R_c), \quad (c = 1, 2) \quad (2.13)$$

where $L_1 = J$, and $u_L^{(\pm)}(k_c R_c) (= G_L(k_c R_c) \pm i F_L(k_c R_c))$ are the asymptotic outgoing and incoming Coulomb wave functions. $S_{1 \rightarrow c}^{L_c}$ is the S -matrix for the transition from the incoming channel ($c = 1$) to the outgoing channel c and v_c is the velocity.

The third term in (2.12), $\Psi_{JM}^{(\text{closed})}$, represents all the closed (virtually excited) channels in the energy range in this work; in other words, this term is responsible for all the asymptotically vanishing amplitudes due to the three-body degrees of freedom that are not included in the first two scattering terms.*) Since $\Psi_{JM}^{(\text{closed})}$ vanishes asymptotically, it is reasonable and useful to expand it in terms of a complete set of L^2 -integrable three-body basis functions, $\{\Phi_{JM,\nu}; \nu = 1 - \nu_{\text{max}}\}$, that are spanned in a finite spatial region (see §2.4):

$$\Psi_{JM}^{(\text{closed})} = \sum_{\nu=1}^{\nu_{\text{max}}} b_{J\nu} \Phi_{JM,\nu}. \quad (2.14)$$

Equations for $\chi_J^{(1)}(R_1)$, $\chi_{L_2}^{(2)}(R_2)$ and the coefficients $b_{J\nu}$ are given by the $\nu_{\text{max}} + 2$ simultaneous equations,^{17),25)}

$$\langle \phi_{00}^{(1)}(\mathbf{r}_1) Y_{JM}(\hat{\mathbf{R}}_1) | H - E_{\text{tot}} | \Psi_{JM} \rangle_{\mathbf{r}_1, \hat{\mathbf{R}}_1} = 0, \quad (2.15)$$

$$\langle [\phi_{l_2}^{(2)}(\mathbf{r}_2) \otimes Y_{L_2}(\hat{\mathbf{R}}_2)]_{JM} | H - E_{\text{tot}} | \Psi_{JM} \rangle_{\mathbf{r}_2, \hat{\mathbf{R}}_2} = 0, \quad (2.16)$$

and

$$\langle \Phi_{JM,\nu} | H - E_{\text{tot}} | \Psi_{JM} \rangle = 0. \quad (\nu = 1 - \nu_{\text{max}}) \quad (2.17)$$

Here, $\langle \rangle_{\mathbf{r}_c, \hat{\mathbf{R}}_c}$ denotes integration over \mathbf{r}_c and $\hat{\mathbf{R}}_c$.

Since $\Phi_{JM,\nu}$ are constructed so as to diagonalize the three-body Hamiltonian as (cf. §2.4)

$$\langle \Phi_{JM,\nu} | H | \Phi_{JM,\nu'} \rangle = E_{J\nu} \delta_{\nu\nu'}, \quad (\nu, \nu' = 1 - \nu_{\text{max}}) \quad (2.18)$$

the coefficients $b_{J\nu}$ can be written, from Eq. (2.17), as

$$b_{J\nu} = \frac{-1}{E_{J\nu} - E_{\text{tot}}} \langle \Phi_{JM,\nu} | H - E_{\text{tot}} | \phi_{00}^{(1)}(\mathbf{r}_1) \chi_{JM}^{(1)}(\mathbf{R}_1) + [\phi_{l_2}^{(2)}(\mathbf{r}_2) \otimes \chi_{L_2}^{(2)}(\mathbf{R}_2)]_{JM} \rangle. \quad (\nu = 1 - \nu_{\text{max}}) \quad (2.19)$$

Using Eqs. (2.15), (2.16) and (2.19), we reach two coupled integro-differential equations for $\chi_J^{(1)}(R_1)$ and $\chi_J^{(2)}(R_2)$, which are not written here (see §8 of Ref. 17) for the equations).

Finally, the integro-differential equations are solved using both the direct numerical method (the finite-difference method) and the Kohn-type variational method.^{17),25)} We obtained the same result; this demonstrates the high accuracy of our three-body calculation.

Using the S -matrix elements obtained above, the cross section of the rearrangement process is expressed as

$$\sigma(E) = \frac{\pi}{k_1^2} \sum_{J=0}^{\infty} (2J+1) |S_{1 \rightarrow 2}^{L_2}|^2. \quad (2.20)$$

*) This method for low-energy three-body reactions has already been used^{17),21)-23)} in the study of the muon transfer reaction $(d\mu)_{1s} + t \rightarrow (t\mu)_{1s} + d + 48 \text{ eV}$. The $\Psi_{JM}^{(\text{closed})}$ term was found to play a very important role; if the term is omitted (namely, if the two-channel coupled calculation is performed with $c = 1, 2$), the calculated low-energy (0.001 – 100 eV) cross section of the reaction becomes ~ 30 times larger than that obtained by the full three-body calculation.

where we introduce a simplified notation, $E \equiv E_1$, for the energy of the entrance channel. The astrophysical S -factor is derived from

$$\sigma(E) = S(E) \exp(-2\pi\eta(E))/E. \quad (2.21)$$

Here, $\exp(-2\pi\eta(E))$ is the Coulomb barrier penetration probability, where $\eta(E)$ is the Sommerfeld parameter of the entrance channel $(AX^-) + a$, defined as

$$\eta(E) = Z_a Z_{AX} e^2 / \hbar v_1, \quad (2.22)$$

where $Z_a e$ and $Z_{AX} e$ are the charges of a and (AX^-) , respectively.

The reaction rate $\langle \sigma v \rangle$ at temperature T is expressed as (cf. Eq. (4-44) of Ref. 26))

$$\langle \sigma v \rangle = \left(\frac{8}{\pi M_1} \right)^{\frac{1}{2}} \frac{1}{(kT)^{\frac{3}{2}}} \int_0^\infty S(E) \exp\left(-\frac{E}{kT} - 2\pi\eta(E)\right) dE, \quad (2.23)$$

where k is the Boltzmann constant. If $S(E)$ is simulated by a linear function of E around the Gamow peak energy E_0 as

$$S(E) \simeq S(E_0) + \left(\frac{\partial S}{\partial E} \right)_{E_0} (E - E_0), \quad (2.24)$$

$$E_0 = 122.0 (Z_a^2 Z_{AX}^2 \mu)^{\frac{1}{3}} T_9^{\frac{2}{3}} \text{ keV}, \quad (2.25)$$

the reaction rate $N_A \langle \sigma v \rangle$ is expressed, using Eqs. (4-56) and (4-75) of Ref. 26), as

$$\begin{aligned} N_A \langle \sigma v \rangle &= 7.82 \times 10^6 \left(\frac{Z_a Z_{AX}}{\mu} \right)^{\frac{1}{3}} \left[S(E_0) + 71.8 \left(\frac{\partial S}{\partial E} \right)_{E_0} T_9 \right] \\ &\times T_9^{-\frac{2}{3}} \exp \left[-4.248 (Z_a^2 Z_{AX}^2 \mu)^{\frac{1}{3}} T_9^{-\frac{1}{3}} \right] \text{ cm}^3 \text{ s}^{-1} \text{ mol}^{-1}, \end{aligned} \quad (2.26)$$

where $S(E_0)$ and $(\partial S/\partial E)_{E_0}$ are given in units of keV b and b, respectively, N_A is Avogadro's number and μ is M_1 in units of amu. As will be seen for any nonresonant reaction in this paper, we can regard $(\partial S/\partial E)_{E_0} \approx \text{constant} \equiv \alpha$:

$$S(E) = S(E_0) + \alpha (E - E_0) = S(0) + \alpha E, \quad (2.27)$$

where $S(0)$ and α are given in units of keV b and b, respectively, and E is in keV. We then have

$$\begin{aligned} N_A \langle \sigma v \rangle &= 7.82 \times 10^6 \left(\frac{Z_a Z_{AX}}{\mu} \right)^{\frac{1}{3}} S(0) T_9^{-\frac{2}{3}} \exp \left[-4.248 (Z_a^2 Z_{AX}^2 \mu)^{\frac{1}{3}} T_9^{-\frac{1}{3}} \right] \\ &\times \left[1 + \frac{\alpha}{S(0)} \left\{ 122.0 (Z_a^2 Z_{AX}^2 \mu)^{\frac{1}{3}} T_9^{\frac{2}{3}} + 71.8 T_9 \right\} \right] \text{ cm}^3 \text{ s}^{-1} \text{ mol}^{-1}. \end{aligned} \quad (2.28)$$

2.3. Nuclear and Coulomb potentials

It is essential in the three-body calculation to employ appropriate interactions among the three particles. Here, we determine the potentials $V_{A-X}(r_1)$, $V_{A-a}(r_2)$ and $V_{a-X}(r_3)$ in (2.9), where $A = \alpha$ and $a = d, t$ and ${}^3\text{He}$.

We assume the Gaussian charge distribution $Ze(\pi b^2)^{-3/2}e^{-(r/b)^2}$ for α , d , t and ${}^3\text{He}$; here, Ze is the charge and $b = \sqrt{2/3}r_0$, where r_0 is the observed rms charge radius, which is given by $r_0 = 1.67, 2.14, 1.70$ and 1.95 fm, respectively.

The Coulomb potential between A and X^- is given by

$$V_{A-X}(r) = -Z_A e^2 \frac{\text{erf}(r/b_A)}{r}, \quad (2.29)$$

where $\text{erf}(x) = \frac{2}{\sqrt{\pi}} \int_0^x e^{-t^2} dt$ is the error function; and the Coulomb potential is similarly defined for $V_{a-X}(r)$. The energy of the $(\alpha X^-)_{1s}$ state is $\varepsilon_{\text{gs}}^{(1)} = -337.3$ keV (-347.6 keV) and the rms radius is 6.84 fm (6.69 fm) for $m_X = 100$ GeV ($m_X \rightarrow \infty$).

The potential $V_{A-a}(r)$ is a sum of the nuclear potential, $V_{A-a}^{\text{N}}(r)$, and the Coulomb potential, $V_{A-a}^{\text{C}}(r)$. The latter is given by

$$V_{A-a}^{\text{C}}(r) = Z_A Z_a e^2 \frac{\text{erf}(r/\sqrt{b_A^2 + b_a^2})}{r}. \quad (2.30)$$

The nuclear potential $V_{A-a}^{\text{N}}(r)$ is assumed to have a two-range Gaussian shape as

$$V_{A-a}^{\text{N}}(r) = v_1 e^{-(r/a_1)^2} + v_2 e^{-(r/a_2)^2}. \quad (2.31)$$

i) α - d potential

We take $a_1 = 0.9$ fm, $v_1 = 500.0$ MeV, $a_2 = 2.0$ fm and $v_2 = -64.06$ MeV.⁵⁾ The first term, a repulsive core, is introduced to simulate the Pauli exclusion principle that nucleons in the incoming deuteron should not occupy the nucleon s -orbit in the α particle during the reaction process (for this role of the Pauli principle,^{*} see, for example, Ref. 27)). The parameters are determined so that the solution to the Schrödinger equation (2.10) for $c = 2$ reproduces observed values of both the energy $\varepsilon_{\text{gs}}^{(2)} = -1.474$ MeV and the rms charge radius 2.54 fm²⁸⁾ of the ground state of ${}^6\text{Li}$. Furthermore, the charge density of ${}^6\text{Li}$ reproduces the observed charge form factor of the electron scattering from ${}^6\text{Li}$ (see Fig. 2 of Ref. 5)). Simultaneously, the use of the potential $V_{\alpha-d}(r_2)$ explains the low-energy s -wave phase shifts of the $\alpha + d$ scattering (see Fig. 2 of Ref. 5)).

ii) α - t potential

The nuclear potential between α and t is assumed to be parity dependent; $a_1 = 1.0$ fm, $v_1 = 500.0$ MeV, $a_2 = 2.7$ fm and $v_2 = -46.22$ MeV for odd angular-momentum

^{*} Use of the sophisticated orthogonality-condition model (OCM)²⁹⁾ for three-body systems is not necessary in the present case, since the Pauli principle only applies between A and a among the three particles, and we are not treating their compact bound states. However, the introduction of the inner repulsive potential is useful in this type of three-body scattering calculation to automatically prevent the unphysical Pauli forbidden amplitude from entering the total wave function.

states and $a_1 = 1.5$ fm, $v_1 = 500.0$ MeV, $a_2 = 2.4$ fm and $v_2 = -7.0$ MeV for even angular-momentum states. The repulsive term is introduced so as to prevent the Pauli forbidden states from entering the total wave function. The use of the potential reproduces the observed energy $\varepsilon_{\text{gs}}^{(2)} = -2.308$ MeV (weighted average for the $3/2^-$ ground state and the $1/2^-$ excited state) and the rms charge radius 2.43 fm²⁸⁾ of the ground state of ${}^7\text{Li}$ as well as the observed values of the low-energy α - t scattering phase shifts for the p -wave (average of the $p_{3/2}$ and $p_{1/2}$ states) and the s -wave.

iii) α - ${}^3\text{He}$ potential

The nuclear α - ${}^3\text{He}$ potential is assumed to have the same shape and parameters as the α - t potential except that $v_2 = -44.84$ MeV for odd states, which reproduces the observed weighted mean energy ($\varepsilon_{\text{gs}}^{(2)} = -1.444$ MeV) of the ground state and the $1/2^-$ excited state.

2.4. Three-body basis functions

The L^2 -integrable three-body basis functions $\{\Phi_{JM,\nu}; \nu = 1 - \nu_{\text{max}}\}$ used in (2.14) to expand $\Psi_{JM}^{(\text{closed})}$ are introduced as follows:¹⁷⁾ $\Phi_{JM,\nu}$ are written as a sum of the component functions in the Jacobi coordinate sets $c = 1 - 3$ (Fig. 1),

$$\Phi_{JM,\nu} = \Phi_{JM,\nu}^{(1)}(\mathbf{r}_1, \mathbf{R}_1) + \Phi_{JM,\nu}^{(2)}(\mathbf{r}_2, \mathbf{R}_2) + \Phi_{JM,\nu}^{(3)}(\mathbf{r}_3, \mathbf{R}_3). \quad (2.32)$$

Each component is expanded in terms of the Gaussian basis functions of \mathbf{r}_c and \mathbf{R}_c :

$$\Phi_{JM,\nu}^{(c)}(\mathbf{r}_c, \mathbf{R}_c) = \sum_{n_{clc}, N_{cLc}} A_{J\nu, n_{clc}, N_{cLc}}^{(c)} [\phi_{n_{clc}}^{\text{G}}(\mathbf{r}_c) \psi_{N_{cLc}}^{\text{G}}(\mathbf{R}_c)]_{JM}, (c = 1 - 3) \quad (2.33)$$

where the Gaussian ranges are postulated to lie in a geometric progression:

$$\phi_{nlm}^{\text{G}}(\mathbf{r}) = r^l e^{-(r/r_n)^2} Y_{lm}(\hat{\mathbf{r}}), \quad r_n = r_1 a^{n-1}, \quad (n = 1 - n_{\text{max}}) \quad (2.34)$$

$$\psi_{NLM}^{\text{G}}(\mathbf{R}) = R^L e^{-(R/R_N)^2} Y_{LM}(\hat{\mathbf{R}}), \quad R_N = R_1 A^{N-1}. \quad (N = 1 - N_{\text{max}}) \quad (2.35)$$

The basis functions chosen in this way are suitable for describing both short-range correlations (mainly due to nuclear interactions) and long-range asymptotic behavior simultaneously, and therefore they are efficient for describing any three-body configuration (the closed-channel contribution) in the interaction region of the intermediate stage of reactions. The coefficients $A_{J\nu, n_{clc}, N_{cLc}}^{(c)}$ in (2.33) and the eigenenergies $E_{J,\nu}$ of $\Phi_{JM,\nu}$ are determined by diagonalizing the three-body Hamiltonian H as (2.18).

This method in which the total Hamiltonian is diagonalized using the precise Gaussian basis functions has successfully been applied to the study of various types of three- and four-body systems in physics,^{*)} which is reviewed in Ref. 17).

i) Basis set for $\alpha + d + X^-$

*) The most precise three-body calculation among the applications is the determination^{17),30)} of the antiproton mass³¹⁾ by analyzing CERN's laser spectroscopic data on the antiprotonic helium atom, $\text{He}^{++} + e^- + \bar{p}$.³²⁾ The energies of the three-body atom with $J \sim 35$ were calculated with an accuracy of 10 significant figures.

In the calculation for $J = 0$, we took $l_c = L_c = 0, 1, 2$ and $n_{\max} = N_{\max} = 15$ for $c = 1 - 3$. The total number of the three-body Gaussian basis $[\phi_{n_c l_c}^G(\mathbf{r}_c) \psi_{N_c L_c}^G(\mathbf{R}_c)]_{JM}$ used to construct the eigenfunctions $\{\Phi_{JM, \nu}\}$ amounts to $\nu_{\max} = 2025$, which was found to be sufficiently large for the present calculation. For the Gaussian ranges, we took $\{r_1, r_{n_{\max}}, R_1, R_{N_{\max}}\} = \{0.5, 15.0, 1.0, 40.0 \text{ fm}\}$, which are sufficiently precise for the present purpose. The expansion (2.14) converges quickly with increasing ν , and $\nu \lesssim 100$ ($E_{J\nu} \lesssim 1$ MeV above the $(\alpha X^-) - d$ threshold) is sufficient for the conversion. Basis sets for $J \geq 1$ are not shown since the contribution to the cross section from $J \geq 1$ is 3 orders of magnitude smaller than that from $J = 0$.

ii) *Basis set for $\alpha + t(^3\text{He}) + X^-$*

Since $l_2 = 1$ in the exit channel of (2.4) and (2.5), the basis $[\phi_{n_c l_c}^G(\mathbf{r}_c) \psi_{N_c L_c}^G(\mathbf{R}_c)]_{JM}$ for $J = 1$ with $\{(l_1 = 0, L_1 = 1), (l_2 = 1, L_2 = 0)\}$ is the most important (see Figs. 3 and 4). The next most important set for $J = 1$ is $\{(l_1 = 1, L_1 = 0), (l_2 = 1, L_2 = 0)\}$. We take Gaussian ranges $\{r_1, r_{n_{\max}}, R_1, R_{N_{\max}}\} = \{0.4, 15.0, 0.8, 30.0 \text{ fm}\}$ with $n_{\max} = N_{\max} = 12$. The contribution of $J = 0$ to the S -factor is several times smaller than that of $J = 1$; we take the set ($l_c = L_c = 0, 1$) for $c = 1 - 3$.

2.5. Result for ^6Li production

In this subsection we study the ^6Li production reaction (2.2) that is the most important CBBN reaction. A three-body calculation of (2.2) was reported in Ref. 5) by Hamaguchi *et al.*, and therefore we simply recapitulate it here. The calculated astrophysical S -factor $S(E)$ is shown in Fig. 2 together with the Gamow peak at $E_0 = 33$ keV for $T_9 = 0.1$ ($kT = 8.62$ keV) around which (αX^-) is formed. The contribution from the s -wave incoming channel with $(l_1 = L_1 = 0) \rightarrow (l_2 = L_2 = 0)$ is dominant and that from the p -wave incoming channel with $(l_1 = 0, L_1 = 1) \rightarrow (l_2 = 0, L_2 = 1)$ is 3 orders of magnitude smaller. A significant effect of the closed-channel amplitude $\Psi_{JM}^{(\text{closed})}$ in (2.12), which represents the contribution of the three-body degree of freedom in the interaction region, can be seen as follows. If the term $\Psi_{JM}^{(\text{closed})}$ is omitted in the three-body calculation, $S(E)$ becomes nearly 3 times smaller than that in Fig. 2.

The CBBN S -factor in Fig. 2 is enhanced by a factor of $\sim 10^7$ compared with that of the SBBN reaction (2.1). This confirms the large enhancement ($\sim 10^8$) pointed out by Pospelov,¹⁾ although his scaling relation for the estimation is too naive. Note that the S -factor in Fig. 2 is of a similar magnitude to that in typical nonresonant photonless SBBN reactions and that the large enhancement ratio originates simply from the fact that the SBBN reaction (2.1) is heavily E1-hindered.

The energy dependence of $S(E)$ in Fig. 2 is approximated by (2.27) with $S(0) = 44.6$ keV b and $\alpha = -0.18$ b. The reaction rate is then given, using (2.28), as^{*)}

$$N_A \langle \sigma v \rangle = 2.78 \times 10^8 T_9^{-\frac{2}{3}} \exp(-5.33 T_9^{-\frac{1}{3}}) (1 - 0.62 T_9^{\frac{2}{3}} - 0.29 T_9) \text{ cm}^3 \text{ s}^{-1} \text{ mol}^{-1} \quad (2.36)$$

^{*)} The expression (2.36) is slightly different from (4.3) in Ref. 5). The latter is for the vicinity of $kT = 10$ keV ($T_9 = 0.116$), while the former is valid for a wider range of $T_9 \lesssim 0.2$.

for $T_9 \lesssim 0.2$. On the other hand, since the SBBN reaction rate of (2.1) is given¹⁸⁾ as

$$N_A \langle \sigma v \rangle_{\text{SBBN}} = 14.8 T_9^{-\frac{2}{3}} \exp(-7.44 T_9^{-\frac{1}{3}}) (1 + 6.57 T_9 + \dots) \text{ cm}^3 \text{ s}^{-1} \text{ mol}^{-1}, \quad (2.37)$$

the CBBN/SBBN ratio of the *reaction rates* is $\sim 10^9$ at $T_9 = 0.1$. This increase of the ratio from that of the *S-factors* ($\sim 10^7$) is due to the reduction of the CBBN Coulomb barrier experienced by the incoming particle (deuteron) in (2.21).

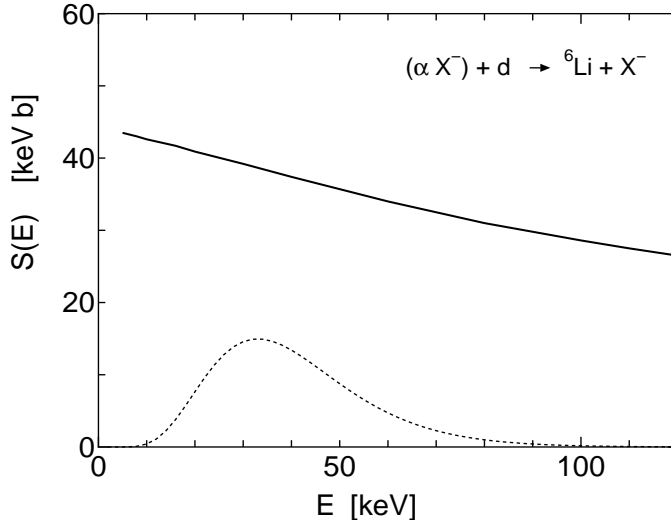


Fig. 2. The astrophysical S -factor of the CBBN reaction (2.2) obtained by the three-body calculation (solid line). The dotted curve (in arbitrary units) illustrates the Gamow peak for $T_9 = 0.1$ ($kT = 8.62$ keV) with the maximum at $E_0 = 33$ keV. This figure is taken from Ref. 5).

It is desirable to quantitatively examine how sensitive the calculated cross section (S -factor) is to the choice of the α - d potential parameter set that reproduces the empirical α - d binding energy and the measured rms charge radius of ${}^6\text{Li}$. We examined this sensitivity by adopting another parameter set $\{r_1 = 0.9$ fm, $V_1 = 400$ MeV, $r_2 = 2.5$ fm, $V_2 = -35.04$ MeV $\}$, which is markedly different from the set shown in §2.4. However, we found that the new result for the S -factor differs by only 5 – 6% from that in Fig. 2. One can expect a similar result for other nonresonant reactions studied in the present paper, although such a test is not repeated there.

So far, the mass of the X^- particle, m_X , has been assumed to be 100 GeV. However, we found that the calculated S -factor differs by only ~ 0.5 % between $m_X = 100$ GeV and $m_X \rightarrow \infty$. Therefore, we take $m_X = 100$ GeV throughout the present paper except for §3, where a resonant reaction is studied.

Using this large CBBN rate (2.36), Hamaguchi *et al.*⁵⁾ solved the evolution equation for the ${}^6\text{Li}$ abundance after SBBN has frozen out. This calculation was performed for various sets of values of the assumed lifetime τ_X and the initial number density n_{X^-} of the X^- particle together with the calculation of the number density of the bound state (αX^-) as a function of the temperature (cf. Fig. 5 of Ref. 5)). For the limiting case of a long lifetime ($\tau_X \gg 1000$ s), they obtained $n_{6\text{Li}}/n_{\text{B}} \simeq$

$3.7 \times 10^{-5} n_{X^-}/n_B$, where $n_{6\text{Li}}$ and n_B are the number densities of ${}^6\text{Li}$ and baryons, respectively. Therefore, the observational upper bound for the ${}^6\text{Li}$ abundance ${}^6\text{Li} < 6.1 \times 10^{-11} (2\sigma)^{33}$ leads to a remarkable bound for the X^- abundance, $n_{X^-}/n_B < 1.6 \times 10^{-6}$. The implication of this result for particle physics is discussed in Ref. 5).

2.6. Result for ${}^7\text{Li}$ and ${}^7\text{Be}$ production

The calculated astrophysical S -factor of the ${}^7\text{Li}$ production reaction (2.4) is shown in Fig. 3. The magnitude of $S(E_0)$ at the Gamow peak energy is approximately one order smaller than that of the ${}^6\text{Li}$ production reaction in Fig. 2. This is because the ground state of ${}^6\text{Li}$ has s -wave ($l_2 = 0$) angular momentum of the d - α configuration whereas that of ${}^7\text{Li}$ has p -wave ($l_2 = 1$) angular momentum between t and α . The incident wave with $l_1 = L_1 = 0$ must cause the angular-momentum rearrangement to $l_2 = L_2 = 1$ in the exit channel, and therefore the most effective partial wave is that with $l_1 = 0, L_1 = 1$ in the incident channel and $l_2 = 1, L_2 = 0$ in

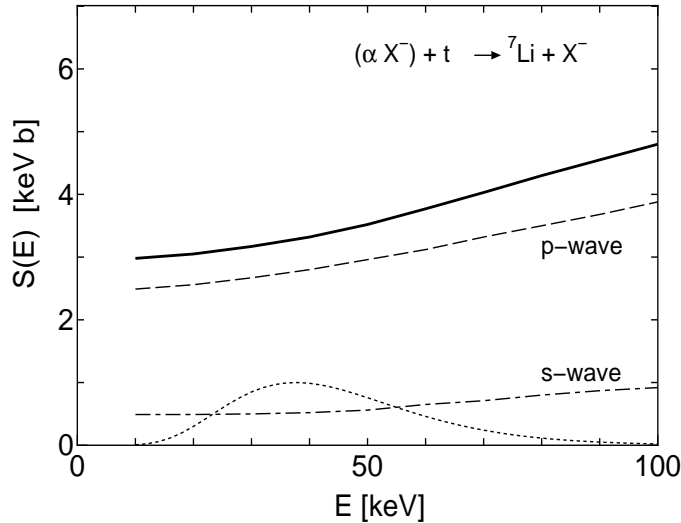


Fig. 3. The S -factor of the CBBN reaction (2.4) obtained by the three-body calculation (the solid line). The s - and p -wave contributions are shown individually. The dotted curve (in arbitrary units) illustrates the Gamow peak for $T_9 = 0.1$ ($kT = 8.6$ keV) with $E_0 = 38$ keV.

the exit channel. This can be seen in Fig. 3; the contribution of the p -wave ($L_1 = 1$) in the incident channel is much larger than that of the s -wave ($L_1 = 0$).

The large effect of the closed-channel amplitude $\Psi_{JM}^{(\text{closed})}$ in (2.12), which represents the contribution of the three-body degree of freedom in the interaction region can be seen as follows. If the term $\Psi_{JM}^{(\text{closed})}$ is omitted in the three-body calculation, $S(E)$ becomes nearly 50 times smaller than that in Fig. 3. The effect changes markedly from the case of ${}^6\text{Li}$ production in §2.5 (namely, from 3 times to 50 times). This is due to the fact that the angular-momentum transfer between the entrance and exit channels is difficult at low energies much lower than the Coulomb barrier, and therefore the transfer is strongly mediated by the degree of three-body distortion in the internal region where the reaction takes place.

In the above calculation, the spin of t is neglected and therefore the $3/2^-$ ground state and $1/2^-$ excited state are degenerated. However, this assumption was found to work well in a more precise calculation with the spin of t and the spin-dependent α - t interaction taken into account explicitly. Namely, the S -factors of the transition to the ground and excited states were found to be, respectively, 53% and 50% of the S -factor by the present spin-neglected calculation (the solid curve in Fig. 3) in the Gamow peak region, and therefore their sum (103%) deviates from the spin-neglected case by only 3%, although the above respective percentages deviate from the numbers 67% and 33% (proportional to the spin weights) in the case where the $3/2^-$ ground and $1/2^-$ excited states are assumed to have the same degenerated binding energy and the same radial wave function.

The magnitude of $S(E)$ for ${}^7\text{Li}$ production in CBBN is approximately 30 times larger than the S -factor of the E1 radiative capture SBBN reaction (2.6) in the Gamow peak region in Fig. 3, $S_\gamma(E_0) \sim 0.1$ keV b.¹⁸⁾ This CBBN/SBBN enhancement factor of ~ 30 is very much smaller than that of $\sim 10^7$ for ${}^6\text{Li}$ production. This is simply because the E1 transition in SBBN is allowed in ${}^7\text{Li}$ production but is heavily hindered in ${}^6\text{Li}$ production. However, as was pointed out in §2.1.2., Cyburt *et al.*⁴⁾ predicted a very large CBBN/SBBN enhancement factor ($\sim 10^5$) assuming the scaling relation.¹⁾ This large overestimation is because the scaling relation, which compares the wavelengths of the real and virtual photons, is not suitable for this type of transfer reaction caused by the strong nuclear interaction. On the other hand, Kusakabe *et al.*¹²⁾ neglected the CBBN processes for the creation of ${}^7\text{Li}$ and ${}^7\text{Be}$ in their BBN network calculation by taking the same consideration as above for the angular-momentum rearrangement ($l_1 = L_1 = 0$) \rightarrow ($l_2 = L_2 = 1$). Although consideration of the largest contribution from ($l_1 = 0, L_1 = 1$) \rightarrow ($l_2 = 1, L_2 = 0$) is missing in Ref. 12), we support their assumption as a reasonable one. However, our reaction rates given below will be employed in the BBN network calculation when the abundances of ${}^7\text{Li}$ and ${}^7\text{Be}$ are precisely discussed.

The energy dependence of $S(E)$ in Fig. 4 may be approximated by expression (2.27) with $S(0) = 2.6$ keV b and $\alpha = 0.02$ b, and therefore the reaction rate is written, for $T_9 \lesssim 0.2$, as

$$N_A \langle \sigma v \rangle = 1.4 \times 10^7 T_9^{-\frac{2}{3}} \exp(-6.08 T_9^{-\frac{1}{3}}) (1 + 1.3 T_9^{\frac{2}{3}} + 0.55 T_9) \text{ cm}^3 \text{ s}^{-1} \text{ mol}^{-1}. \quad (2.38)$$

The calculated S -factor for the ${}^7\text{Be}$ production reaction (2.5), is shown in Fig. 4. Almost the same discussion as that for ${}^7\text{Li}$ production can be made. The S -factor $S(E)$ in Fig. 4 may be approximated with $S(0) = 13.7$ keV b and $\alpha = 0.01$ b, then the reaction rate is written, for $T_9 \lesssim 0.2$, as

$$N_A \langle \sigma v \rangle = 9.4 \times 10^7 T_9^{-\frac{2}{3}} \exp(-9.66 T_9^{-\frac{1}{3}}) (1 + 0.20 T_9^{\frac{2}{3}} + 0.05 T_9) \text{ cm}^3 \text{ s}^{-1} \text{ mol}^{-1}. \quad (2.39)$$

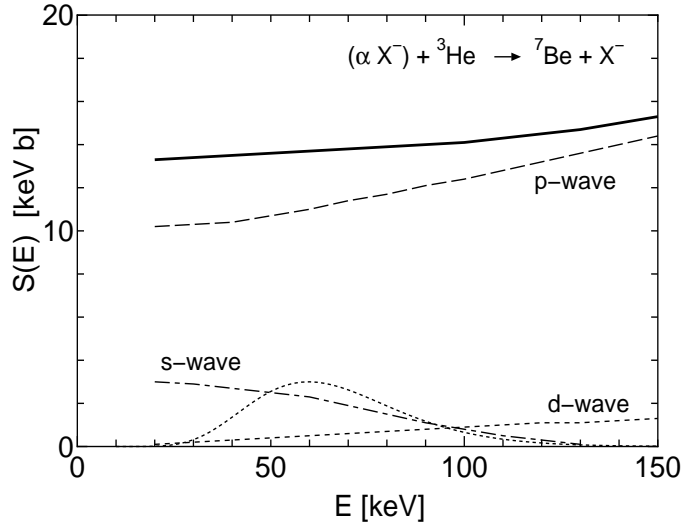


Fig. 4. The S -factor of the CBBN reaction (2.5) obtained by the three-body calculation (solid line). The s -, p - and d -wave contributions are shown individually. The dotted curve (in arbitrary units) illustrates the Gamow peak for $T_9 = 0.1$ ($kT = 8.6$ keV) with $E_0 = 60$ keV.

§3. X^- -catalyzed radiative capture reactions

3.1. Necessity of three-body calculation

Since the $A = 7$ nuclei dominantly produced are ${}^7\text{Be}$ (eventually decaying to ${}^7\text{Li}$ by electron capture) in the BBN network calculation with the CMB-based $\eta_{\text{B}} = 6.0 \times 10^{-10}$, any reaction^{*)} that destroys ${}^7\text{Be}$ might be effective in reducing the overproduction of ${}^7\text{Li}$. For this purpose, Bird *et al.*⁶⁾ considered a resonant radiative capture reaction (cf. Fig. 5),



where the intermediate state, denoted as $({}^8\text{B}X^-)_{2p}^{(\text{res})}$, is a Feshbach resonance generated by the coupling of the atomic $2p$ excited state, say $({}^8\text{B}X^-)_{2p}$, with the $({}^7\text{Be}X^-) + p$ continuum. Here, note that after rapid β -decay, the bound state $({}^8\text{B}X^-)$ transforms to $({}^8\text{Be}(2^+, 3 \text{ MeV})X^-)$, which immediately decays^{**)} to the scattering channel $\alpha + \alpha + X^- + 1.5 \text{ MeV}$.

Assuming a simple Gaussian charge distribution of the ${}^8\text{B}$ nucleus, Bird *et al.* calculated the energy of $({}^8\text{B}X^-)_{2p}$, E_{2p} , with respect to the ${}^8\text{B} + X^-$ threshold. They obtained $E_{2p} = -1.026 \text{ MeV}$ and estimated the resonance energy, E_{res} , with respect to the $({}^7\text{Be}X^-) + p$ threshold as $E_{\text{res}} = E_{2p} + E_{s\text{B}} - E_{({}^7\text{Be}X^-)} = 0.167 \text{ MeV}$ without

^{*)} The reaction $({}^7\text{Be}X^-) + p \rightarrow {}^8\text{B} + X^-$ is energetically impossible due to the negative Q -value (-1.323 MeV); note that the binding energy of ${}^8\text{B}$ is only 0.138 MeV .

^{**)} The authors of Refs. 6) and 14) erroneously consider that $({}^8\text{B}X^-)$ transforms to $({}^8\text{Be}(\text{gs})X^-)$ and that the latter state could potentially lead to a new primordial source of ${}^9\text{Be}$ via $({}^8\text{Be}X^-) + n \rightarrow {}^9\text{Be} + X^-$. Note that ${}^8\text{B}$ shows no β -decay to ${}^8\text{Be}(\text{gs})$.

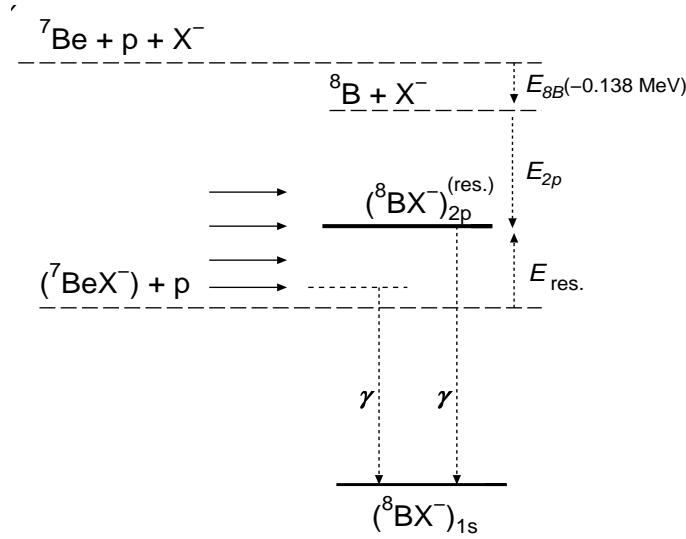
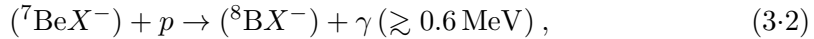


Fig. 5. Schematic illustration of the X^- -catalyzed resonant and nonresonant radiative capture processes (3-1) and (3-2).

the scattering calculation. Further assuming that the resonance width Γ_{res} is much larger than the radiative width for decay to $({}^8\text{BX}^-)_{1s}$, they derived the reaction rate of (3-1) and claimed that the resonant reaction (3-1) is effective in reducing the ${}^7\text{Li}$ - ${}^7\text{Be}$ abundance in their BBN network calculation⁶⁾ and in restricting the lifetime and primordial abundance of the X^- particle.

As discussed below, the rate of the resonant reaction depends strongly on E_{res} , but the model in Ref. 6) is too simple to treat the resonance state. Therefore, in this section, we perform a precise ${}^7\text{Be} + p + X^-$ three-body scattering calculation of the resonant reaction (3-1) as well as the nonresonant radiative capture reaction



although the reaction rate of (3-2) is much smaller than that of (3-1).

Since the rate of the resonant reaction is proportional to $\exp(-E_{\text{res}}/kT)$, a small change in E_{res} can generate a large change in the rate; for example, at $T_9 = 0.3$ ($kT = 25 \text{ keV}$), increase (decrease) of 50 keV in E_{res} changes the reaction rate by a factor of $e^2 (= 7.4)$. The 50 keV change is only 5% of the binding energy ($-E_{2p} \sim 1.0 \text{ MeV}$) of the $({}^8\text{BX}^-)_{2p}$ state, and therefore it is essential to calculate E_{res} with the detailed structure of the ${}^8\text{B}$ nucleus taken into account.

Since the nucleus ${}^8\text{B}$ has been extensively studied, mainly from the viewpoint of the physics of unstable nuclei and that of the solar neutrino problem, a large amount of information about ${}^8\text{B}$ has been accumulated.^{28), 34)-39)} The ground state of ${}^8\text{B}$, being very weakly bound ($E_{8\text{B}} = -0.138 \text{ MeV}$) with respect to the ${}^7\text{Be} + p$ threshold, is known to have a p -wave proton *halo* (a long-range tail) with the ${}^7\text{Be} + p$ structure. Therefore, as will be shown below, the charge distribution of ${}^8\text{B}$ has a long-range *quadrupole* component, which generates the anisotropic part of the Coulomb potential between ${}^8\text{Be}$ and X^- . The expectation values of this part for

the $({}^8\text{B}X^-)_{2p}$ wave function amount to some -50 keV ($J = 0$), $+10$ keV ($J = 1$) and $+30$ keV ($J = 2$), where J denotes the total angular momentum, to which the p -wave ${}^7\text{Be} - p$ relative motion in ${}^8\text{B}$ and the p -wave relative motion between ${}^8\text{B}$ and X^- are coupled (see (3-3) below).

Another important factor that we have to consider concerning ${}^8\text{B}$ is the spins of the ${}^7\text{Be}$ ($3/2^-$) core and the valence proton ($1/2$). The two spins couple with the p -wave angular momentum between ${}^7\text{Be}$ and p to give the total angular momentum of 2^+ in the ground state. The other possible spin-coupling states are not bound; the excitation energies of the 1^+ and 3^+ resonance states are 0.77 and 2.32 MeV, respectively. Therefore, we cannot neglect the fact that the ground state of ${}^8\text{B}$ has the specific spin of 2^+ .

However, the estimation of E_{2p} in Ref. 6) was made assuming an isotropic Gaussian form of the charge distribution of ${}^8\text{B}$ with neither the ${}^7\text{Be} + p$ structure nor the spins of the particles taken into account. In this section, we investigate reactions (3-1) and (3-2), explicitly adopting the ${}^7\text{Be} + p + X^-$ three-body degree of freedom in which the very diffuse, anisotropic charge distribution of ${}^8\text{B}$ ($= {}^7\text{Be} + p$) is automatically taken into account. The use of this three-body model makes it possible to calculate not only the precise resonance energy E_{res} but also the cross section of the first transition process in (3-1), which could not be treated by the model of structureless ${}^8\text{B}$ in Ref. 6).

3.2. Resonance energy obtained using approximate models of ${}^8\text{B}$

Before performing the three-body calculation, we employ four types of approximate models of ${}^8\text{B}$, Models i) to iv) below, and discuss how the energy of the $({}^8\text{B}X^-)_{2p}$ state, E_{2p} , depends on the assumed structure of ${}^8\text{B}$, although we do not couple the state to the ${}^7\text{Be} + p$ scattering state. This may be an instructive guide to the sophisticated three-body scattering calculation in §§3.3 and 3.4.

Model i) Bird *et al.*⁶⁾ assumed a Gaussian charge distribution of ${}^8\text{B}$ with an rms charge radius of 2.64 fm. This gives $E_{2p} = -1.026$ MeV ($m_X \rightarrow \infty$ is taken throughout this subsection), which corresponds to a resonance energy of $E_{\text{res}}^{(i)} = 167$ keV above the $({}^7\text{Be}X^-) + p$ threshold at -1.330 MeV with respect to the ${}^7\text{Be} + X^- + p$ three-body breakup threshold (see Fig. 5). however, this assumption of the Gaussian charge density is not appropriate for this special nucleus ${}^8\text{B}$.

Model ii) The ${}^8\text{B}$ nucleus is known to have a very loosely bound ${}^7\text{Be} + p$ structure with a p -wave proton halo around the ${}^7\text{Be}$ core.³⁵⁾⁻³⁸⁾ Neglecting the spins of ${}^7\text{Be}$ ($3/2^-$) and the valence proton ($1/2^-$), we firstly calculate the p -state ${}^7\text{Be} - p$ wave function using the most well known ${}^7\text{Be} - p$ potential³⁸⁾ (parameters are given in §3.3). By assuming the charge density of ${}^7\text{Be}$ (proton) to be the Gaussian with the observed rms charge radius of 2.52 fm²⁸⁾ (0.8750 fm³¹⁾), we calculate the charge density of the ground state of ${}^8\text{B}$. Owing to the p -state wave function, the density has both an isotropic monopole part and a deformed quadrupole part. The former is illustrated in Fig. 6 together with the contributions from ${}^7\text{Be}$ and p . The density significantly deviates from the Gaussian shape in the tail region owing to the proton halo. If we take the ${}^8\text{B} - X^-$ Coulomb potential due to the monopole charge density alone,

we have $E^{(\text{mono})}(2p) = -1.009$ MeV, which corresponds to $E_{\text{res}}^{(\text{ii})} = 184$ keV. This increase of E_{res} by 17 keV, compared with 167 keV in Model i), *reduces* the reaction rate of (3.1) by a factor of 2 at $T_9 = 0.3$.

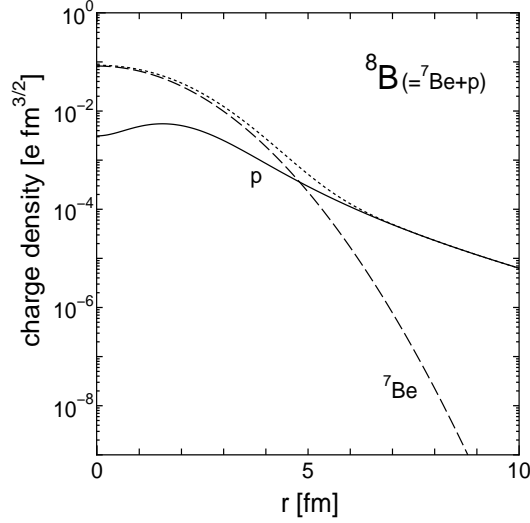


Fig. 6. Monopole part of the charge density, $\rho(r)$, of ${}^8\text{B}$ (dotted line) calculated using the ${}^7\text{Be} + p$ model. The solid (dashed) line shows the contribution from the proton (${}^7\text{Be}$). $\rho(r)$ is normalized as $\int \rho(r) dr = 5$, r being the distance measured from the cm of ${}^8\text{B}$.

Model iii) Using the above Model ii), we further consider the contribution from the quadrupole part of the charge density of ${}^8\text{B}$. Let $\phi_{1m}(\mathbf{r}_2)$ and $\psi_{1M}(\mathbf{R}_2)$ denote the wave functions of the p -wave ${}^8\text{B}$ ground state and the atomic $2p$ relative motion between ${}^8\text{B}$ and X^- , which have already been obtained in Model ii). Then,

$$\Psi_{JM}^{(\text{iii})} = [\phi_1(\mathbf{r}_2) \otimes \psi_1(\mathbf{R}_2)]_{JM} \quad (J = 0, 1, 2) \quad (3.3)$$

is the total wave function of the $({}^8\text{B}X^-)_{2p}$ state^{*)} with angular momentum J and z -component M . The quadrupole part of the Coulomb potential between ${}^8\text{B}$ and X^- , which is sensitive to the angle between \mathbf{r}_2 and \mathbf{R}_2 , should contribute to the total energy dependently on the angular momentum coupling to J . The expectation value of the Hamiltonian with respect to $\Psi_{JM}^{(\text{iii})}$, say $E_J^{(\text{iii})}(2p)$, is written as

$$E_J^{(\text{iii})}(2p) = E^{(\text{mono})}(2p) + \Delta E_J^{(\text{quad})}(2p), \quad (3.4)$$

where $\Delta E_J^{(\text{quad})}(2p)$ is the contribution from the quadrupole part of the charge density of ${}^8\text{B}$ mentioned above and $E^{(\text{mono})}(2p)$ was given in Model ii). We obtain $\Delta E_J^{(\text{quad})}(2p) = -54$ keV ($J = 0$), $+27$ keV ($J = 1$) and -5.4 keV ($J = 2$), and therefore, $E_J^{(\text{iii})}(2p) = -1.063$ keV ($J = 0$), -1.036 keV ($J = 1$) and -1.014 keV ($J = 2$),

^{*)} In this notation of $({}^8\text{B}X^-)_{2p}$ in Model iii), and similarly in Model iv), the p -wave angular momentum of ${}^8\text{B}$ and the total angular momentum J are not explicitly written for simplicity.

which correspond to $E_{\text{res}}^{(\text{iii})} = 130 \text{ keV}$ ($J = 0$), 211 keV ($J = 1$) and 179 keV ($J = 2$). In the case of $J = 0$, the resonance energy, $E_{\text{res}} = 130 \text{ MeV}$, results in a reaction rate that is 8 times larger than that of Model ii). However, we have not yet included the effect of the spins of ${}^7\text{Be}$ ($3/2^-$), p ($1/2$) and ${}^8\text{B}$ (2^+).

Model iv) The spin-parity of the ground state of ${}^8\text{B}$ is 2^+ . In previous studies on ${}^8\text{B}$ taking the ${}^7\text{Be} + p$ model, the structure of low-lying states of ${}^8\text{B}$ is considered as follows: The valence proton is located in the $p_{3/2}$ orbit around the ${}^7\text{Be}$ ($3/2^-$) core, and the two $3/2^-$ spins are coupled to the total angular momentum $I = 2^+$ in the ground state and $I = 1^+$ and 3^+ in the excited states with the observed $E_x = 0.77$ and 2.32 MeV , respectively. Since the spin-dependent interaction is strong and the Coulomb interaction between ${}^8\text{B}$ and X^- does not change the spin structure, we have to seriously consider the ground-state spin 2^+ and its coupling scheme in the calculation of the resonance energy. Let $\phi_{\{p_{3/2}, 3/2\}I}(\mathbf{r}_2)$ denote the wave function of the ground state ($I = 2$) of ${}^8\text{B}$ explained above. The total wave function of the $({}^8\text{B}X^-)_{2p}$ state is written as

$$\Psi_{JM}^{(\text{iv})} = \left[\phi_{\{p_{3/2}, 3/2\}I}(\mathbf{r}_2) \otimes \psi_1(\mathbf{R}_2) \right]_{JM}, \quad (3.5)$$

where $\psi_1(\mathbf{R}_2)$ was given in Model ii). The expectation value of the Hamiltonian with respect to $\Psi_{JM}^{(\text{iv})}$, say $E_{J,I}^{(\text{iv})}(2p)$, is described by the form

$$E_{J,I}^{(\text{iv})}(2p) = E^{(\text{mono})}(2p) + \sum_{\Lambda=0}^2 a_{J,I\Lambda} \Delta E_{\Lambda}^{(\text{quad})}(2p), \quad (3.6)$$

where $E^{(\text{mono})}(2p)$ and $\Delta E_{\Lambda}^{(\text{quad})}(2p)$ are given in (3.4), and $a_{J,I\Lambda}$ is written as

$$a_{J,I\Lambda} = \frac{1}{2}(2J+1)(2\Lambda+1) \sum_{S=1}^2 [W(1I\Lambda J; S1)]^2. \quad (3.7)$$

The second term of Eq. (3.6) vanishes owing to the summation over S for the ground-state spin $I = 2$ but not for $I \neq 2$. We then have $E_{J,I}^{(\text{iv})}(2p) = E^{(\text{mono})}(2p) = -1.009 \text{ MeV}$ for $I = 2^+$, and therefore $E_{\text{res}}^{(\text{iv})} = 184 \text{ MeV}$ ($J = 1, 2$) which is, by chance, the same as in Model ii).

3.3. Three-body calculation of resonance energy and width

In the four types of approximate models for $({}^8\text{B}X^-)_{2p}$ in the previous subsection, ${}^8\text{B}$ is assumed to be the same as that in the free space. However, since ${}^8\text{B}$ is a very loosely bound state of ${}^7\text{Be}$ and p , it is possible that the spatial structure of ${}^8\text{B}$ changes in the presence of X^- , namely, in the presence of the Coulomb potential between ${}^7\text{Be}$ and X^- and that between p and X^- (the spin structure is not changed by these Coulomb potentials). Therefore, using the ${}^7\text{Be} + p + X^-$ three-body model with the Hamiltonian (2.9), we calculate the resonance state as a Feshbach resonance embedded in the $({}^7\text{Be}X^-) + p$ continuum and precisely determine the energy and width of the resonance.

3.3.1. Nuclear and Coulomb potentials

In the ${}^7\text{Be} + p$ model, we treat ${}^7\text{Be}$ as an inert core with spin $3/2^-$. We assume Gaussian charge distributions of ${}^7\text{Be}$ and the proton as $4e(\pi b_{\text{Be}}^2)^{-3/2}e^{-(r/b_{\text{Be}})^2}$ and $e(\pi b_p^2)^{-3/2}e^{-(r/b_p)^2}$, respectively, and take $b_{\text{Be}} = 2.06$ fm and $b_p = 0.714$ fm to reproduce the observed rms charge radii, 2.52 fm²⁸⁾ for ${}^7\text{Be}$ and 0.8750 fm³¹⁾ for the proton. The Coulomb potential between ${}^7\text{Be}$ and X^- is then given by

$$V_{7\text{Be}-X}(r) = -4e^2 \frac{\text{erf}(r/b_{\text{Be}})}{r}, \quad (3.8)$$

and that between X^- and p is written as

$$V_{p-X}(r) = -e^2 \frac{\text{erf}(r/b_p)}{r}. \quad (3.9)$$

The energy of $({}^7\text{Be}X^-)_{1s}$ is $\varepsilon_{\text{gs}}^{(1)} = -1.386$ (-1.324) MeV and the rms radius is 3.60 (3.49) fm for $m_X = 100$ GeV ($m_X \rightarrow \infty$).

The potential $V_{7\text{Be}-p}(r)$ is a sum of the nuclear potential, $V_{7\text{Be}-p}^{\text{N}}(r)$, and the Coulomb potential, $V_{7\text{Be}-p}^{\text{C}}(r)$. The latter is given by

$$V_{7\text{Be}-p}^{\text{C}}(r) = 4e^2 \frac{\text{erf}(r/\sqrt{b_{\text{Be}}^2 + b_p^2})}{r}. \quad (3.10)$$

For the nuclear potential $V_{7\text{Be}-p}^{\text{N}}(r)$ between ${}^7\text{Be}$ and p , we follow the work of Ref. 38), which is a standard study on the ${}^7\text{Be} + p \rightarrow {}^8\text{B} + \gamma$ reaction. The nuclear potential is parameterized as a Woods-Saxon potential plus a spin-orbit potential with an adjustable depth $V_0(lj, I)$:

$$V_{7\text{Be}-p}^{\text{N}}(r) = \left[1 - F_{\text{so}}(\mathbf{l} \cdot \mathbf{s}) \frac{r_0}{r} \frac{d}{dr} \right] \frac{V_0(lj, I)}{1 + \exp[(r - R_0)/a]}. \quad (3.11)$$

Here, we take $a = 0.52$ fm, $R_0 = 2.391$ fm and $F_{\text{so}} = 0.351$ fm.³⁸⁾ The orbital and total angular momenta of the proton are denoted by (lj) . The $I = 2^+$ ground state of ${}^8\text{B}$ is described in terms of a pure $(lj) = p_{3/2}$ orbit of the proton coupled with the $3/2^-$ spin of the ${}^7\text{Be}$ core. The well depth V_0 ($l = 1, j = 3/2, I = 2$) is adjusted to reproduce the binding energy of 0.1375 MeV of the ground state and is given by -44.147 MeV. The s -wave potential between ${}^7\text{Be}$ and p is assumed to have $V_0 = -30.0$ MeV, $R_0 = 2.39$ fm and $a = 0.65$ fm and additionally have a Pauli repulsive potential with $V_0 = 800$ MeV, $R_0 = 1.5$ fm and $a = 0.2$ fm. This s -wave potential gives no bound state.

3.3.2. Resonance wave function

Let $\xi_{\frac{3}{2}}({}^7\text{Be})$ and $\xi_{\frac{1}{2}}(p)$ denote the spin functions of the ${}^7\text{Be}$ ground state and the proton, respectively. The $1s$ ground state of $({}^7\text{Be}X^-)$ is described by $\phi_{00}^{(1)}(\mathbf{r}_1)$. We consider the s -state relative wave function between the incident proton and the target $({}^7\text{Be}X^-)$, say $\chi_{00}^{(1)}(\mathbf{R}_1)(= \chi_0^{(1)}(R_1)Y_{00}(\hat{\mathbf{R}}_1))$, since that of the p -state has a

different parity and that of the d -state has negligible contribution to the resonant radiative capture process. There are neither inelastically excited channels in $c = 1$ nor transfer channels in $c = 2$ and 3 for the energies (< 200 keV) concerned here. The total wave function used to describe the resonant state is then written as

$$\Psi_{JM} = \phi_{00}^{(1)}(\mathbf{r}_1) \chi_{00}^{(1)}(\mathbf{R}_1) \left[\xi_{\frac{3}{2}}({}^7\text{Be}) \otimes \xi_{\frac{1}{2}}(p) \right]_{JM} + \Psi_{JM}^{(\text{closed})}. \quad (3.12)$$

The second term of (3.12), $\Psi_{JM}^{(\text{closed})}$, represents the internal amplitude of the resonance wave function, whose approximate expression is $\Psi_{JM}^{(\text{iv})}$ in (3.5). However, we describe $\Psi_{JM}^{(\text{closed})}$ taking the three-body degrees of freedom in the same way as in §2.4. Since we find that, in (3.12), the contributions from the amplitudes with $c = 1$ and 3 are negligible in the resonance energy region, we here express $\Psi_{JM}^{(\text{closed})}$ as

$$\Psi_{JM}^{(\text{closed})} = \sum_{\nu=1}^{\nu_{\max}} b_{J\nu} \Phi_{JM,\nu}^{(2)} \quad (3.13)$$

using the three-body basis functions only in $c = 2$ together with the spin functions,

$$\Phi_{JM,\nu}^{(2)} = \sum_{n_2, N_2} A_{J\nu, n_2, N_2}^{(2)} \left[[[\phi_{n_2 l_2}^{\text{G}}(\mathbf{r}_2) \otimes \xi_{\frac{1}{2}}(p)]_{\frac{3}{2}} \otimes \xi_{\frac{3}{2}}({}^7\text{Be})]_I \otimes \psi_{N_2 L_2}^{\text{G}}(\mathbf{R}_2) \right]_{JM}, \quad (3.14)$$

where $l_2 = L_2 = 1, I = 2$ and $J = 1, 2$ are sufficient to describe the resonant reaction. For the Gaussian ranges in (2.34) and (2.35), we take $n_{\max} = N_{\max} = 15$ ($\nu_{\max} = 225$) and $\{r_1, r_{n_{\max}}, R_1, R_{N_{\max}}\} = \{0.4, 15.0, 0.6, 20 \text{ fm}\}$, which is sufficiently precise for the present purpose.

By diagonalizing the Hamiltonian, we obtain eigenstates $\{\Phi_{JM,\nu}; \nu = 1 - \nu_{\max}\}$, among which the energy of the lowest-lying state ($\Phi_{JM,\nu=1}$) measured from the ${}^7\text{Be} + p$ threshold is 198, 186, 177 and 174 keV for $m_X = 50, 100$ and 500 GeV and $m_X \rightarrow \infty$, respectively ($J = 1, 2$). The m_X dependence of the energies comes from the fact that the kinetic energy and the ${}^7\text{Be} + p$ threshold energy depend on m_X .

The total wave function (3.12) is solved under the scattering boundary condition

$$\lim_{R_1 \rightarrow \infty} R_1 \chi_0^{(1)}(R_1) = u_0^{(-)}(k_1, R_1) - S_{1 \rightarrow 1}^J u_0^{(+)}(k_1, R_1) \quad (3.15)$$

on the basis of the same prescription as that in §2.2. The resonance state should appear around the energy of the pseudostate $\Phi_{JM,\nu=1}$ mentioned above. The calculated partial-wave elastic scattering cross section is illustrated in Fig. 7 for $J = 1^-$ with $m_X = 50, 100$ and 500 GeV and $m_X \rightarrow \infty$; similar behaviour is obtained for the resonance with $J = 2^-$. The energy E_{res}^J and the proton width Γ_p^J of the resonance are summarized in Table I.

3.4. Result for the resonant radiative capture

The final state, (${}^8\text{B}X^-$), of the radiative reactions (3.1) and (3.2) is obtained as the ground state of the ${}^7\text{Be} + p + X^-$ system. The dominant component is obviously the product of the 2^+ ground-state wave function of ${}^8\text{B}$ and the $1s$ wave function of

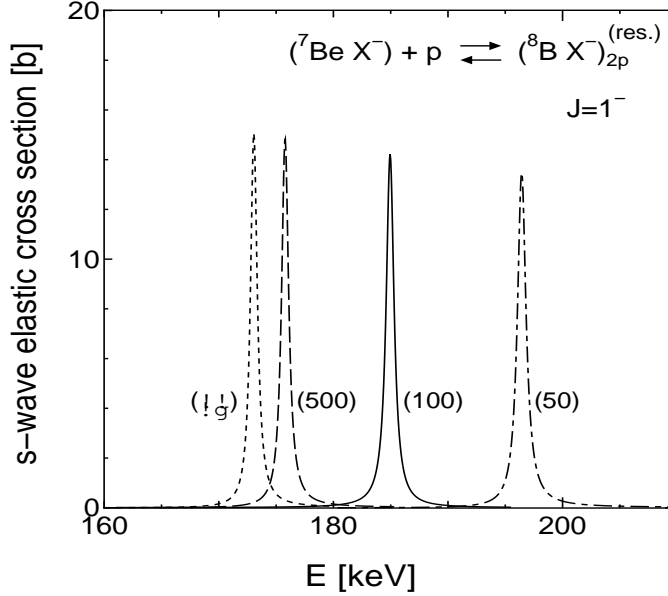


Fig. 7. Partial-wave ($J = 1^-$, s -wave) cross section of the elastic $({}^7\text{Be}X^-)_{1s} + p$ scattering near $({}^7\text{Be}X^-)_{2p}^{\text{res}}$ for the cases of $m_X = 50$ GeV (dash-dotted line), 100 GeV (solid line), 500 GeV (dashed line) and $m_X \rightarrow \infty$ (short dashed line). Similar behaviour is seen for $J = 2^-$ (s -wave).

$({}^8\text{B}X^-)$. We describe it more precisely using the same three-body basis functions in (3.14) with $l_2 = 1, L_2 = 0, I = 2$ and $J = 2$ with the same ranges of the Gaussian basis. Other configurations are not necessary within the accuracy required for the present purpose. By diagonalizing the three-body Hamiltonian, we obtained the ground-state wave function, $\Phi_{J=2+M}^{(\text{gs})}$ and its energy E_{gs} , which is listed in the second to last column of Table I.

The width of the electric dipole (E1) transition from the resonance state $\Psi_{JM}^{(\text{res})}$ with J^- to the 2^+ ground state is given by

$$\Gamma_\gamma^J = \frac{16\pi k_\gamma^3}{9} \frac{1}{2J+1} \sum_{MM'\mu} |\langle \Phi_{2M'}^{(\text{gs})} | Q_{1\mu}^{(E1)} | \Psi_{JM}^{(\text{res})} \rangle|^2, \quad (J = 1, 2) \quad (3.16)$$

where the E1 operator $Q_{1\mu}^{(E1)}$ is defined by

$$Q_{1\mu}^{(E1)} = \sum_{i=1}^3 q_i R_i^G Y_{1\mu}(\hat{\mathbf{R}}_i^G). \quad (3.17)$$

Here q_i and \mathbf{R}_i^G are the i -th particle's charge and its position vector relative to the cm of the total system, respectively, and k_γ is the photon wave number. The calculated values of Γ_γ^J are listed in Table I; they are, as expected, close to the width (10.4 eV) given by the simple atomic E1 transition $({}^8\text{B}X^-)_{2p} \rightarrow ({}^8\text{B}X^-)_{1s}$.

Finally, the reaction rate of the resonant radiative capture process is given using

Table I. The ${}^7\text{Be} + X^- + p$ three-body calculation of the energy (E_{res}), the proton decay width (Γ_p) and the radiative decay width (Γ_γ) of the resonance states with $J = 1^-$ and $J = 2^-$ as well as the energy (E_{gs}) of the three-body ground state with $J = 2^+$. E_{res} and E_{gs} are measured from the $({}^7\text{Be}X^-)_{1s} + p$ threshold, whose energy (E_{th}) is given in the last column with respect to the three-body breakup threshold. All results are calculated for $m_X = 50, 100$ and 500 GeV and $m_X \rightarrow \infty$.

m_X [GeV]	$J = 1^-$ (res)			$J = 2^-$ (res)			$J = 2^+$ (gs)	threshold
	E_{res}^J [keV]	Γ_p^J [keV]	Γ_γ^J [eV]	E_{res}^J [keV]	Γ_p^J [keV]	Γ_γ^J [eV]	E_{gs} [keV]	E_{th} [keV]
50	196.4	0.90	9.1	196.9	0.55	9.1	-624.2	(-1252.0)
100	185.0	0.82	9.6	185.5	0.50	9.6	-635.5	(-1286.1)
500	175.8	0.74	9.9	176.3	0.44	9.9	-643.6	(-1316.4)
∞	173.0	0.71	10.1	173.6	0.43	10.1	-645.9	(-1324.0)

the formula for the reaction (Eq. (4-194) in Ref. 26)) as

$$N_A \langle \sigma v \rangle = N_A \hbar^2 \left(\frac{2\pi}{M_1 kT} \right)^{\frac{3}{2}} \sum_{J=1}^2 \frac{2J+1}{(2I_1+1)(2I_2+1)} \frac{\Gamma_p^J \Gamma_\gamma^J}{\Gamma_p^J + \Gamma_\gamma^J} \exp\left(-\frac{E_{\text{res}}^J}{kT}\right), \quad (3-18)$$

where I_1 and I_2 are the spins of ${}^7\text{Be}$ (3/2) and p (1/2), respectively. Here, we consider that the total width of the resonance, Γ_{res} , is given by $\Gamma_p^J + \Gamma_\gamma^J$ since there is no other decaying channel. We replace the resonance energies E_{res}^J ($J = 1, 2$) by their average, since they are almost the same. We then obtain (in units of $\text{cm}^3 \text{s}^{-1} \text{mol}^{-1}$)

$$N_A \langle \sigma v \rangle = 1.37 \times 10^6 T_9^{-\frac{3}{2}} \exp(-2.28/T_9), \quad (m_X = 50 \text{ GeV}) \quad (3-19)$$

$$N_A \langle \sigma v \rangle = 1.44 \times 10^6 T_9^{-\frac{3}{2}} \exp(-2.15/T_9), \quad (m_X = 100 \text{ GeV}) \quad (3-20)$$

$$N_A \langle \sigma v \rangle = 1.48 \times 10^6 T_9^{-\frac{3}{2}} \exp(-2.04/T_9), \quad (m_X = 500 \text{ GeV}) \quad (3-21)$$

$$N_A \langle \sigma v \rangle = 1.51 \times 10^6 T_9^{-\frac{3}{2}} \exp(-2.01/T_9). \quad (m_X \rightarrow \infty) \quad (3-22)$$

The m_X dependence of the rates is not negligible since, at $T_9 = 0.3$, their ratio is $0.37 : 0.60 : 0.88 : 1.0$ for $m_X = 50, 100$ and 500 GeV and $m_X \rightarrow \infty$. The rate given by Bird *et al.* in the second part of Eq. (3-22) in Ref. 6) for $m_X \rightarrow \infty$ is by chance close to the above rate (3-22); at $T_9 = 0.3$, their rate is 1.2 times that of ours, although the models are markedly different from each other.

3.5. Result for the nonresonant radiative capture

In this subsection, we investigate the nonresonant (direct) radiative capture process (3-2) using the ${}^7\text{Be} + p + X^-$ three-body model. Here, we ignore the intrinsic spins of ${}^7\text{Be}$ and p because, as will be shown below, the calculated reaction rate

without the spins is 4 orders of magnitude smaller than that of the resonant reaction (3.1). The further inclusion of the spins will not change the result meaningfully.

We consider the nonresonant E1 radiative capture from the $J = 0$ incoming state of the $({}^7\text{Be}X^-) + p$ channel to the $J = 1$ ground state in which the ${}^7\text{Be}$ and p are dominantly in p -wave relative motion (other partial-wave states are negligible), and we denote the wave functions respectively as $\Psi_{00}(E)$ and $\Phi_{1M}^{(\text{gs})}$ with the proper normalization. The wave functions can be obtained using the same methods as those in the previous subsections, but the second term of (3.12) can be neglected for the present nonresonant scattering wave.

The cross section of the E1 capture is given by

$$\sigma_{\text{cap}}^{(\text{E1})}(E) = \frac{16\pi}{9} \frac{k_\gamma^3}{\hbar v_1} \sum_M |\langle \Phi_{1M}^{(\text{gs})} | Q_{1M}^{(\text{E1})} | \Psi_{00}(E) \rangle|^2, \quad (3.23)$$

where k_γ is the wave number of the emitted photon and v_1 is the velocity of the relative motion between $({}^7\text{Be}X^-)$ and p .

The calculated $S(E)$ of the CBBN reaction (3.2) is illustrated in Fig. 8 together with the observed S -factor¹⁸⁾ of the SBBN partner reaction

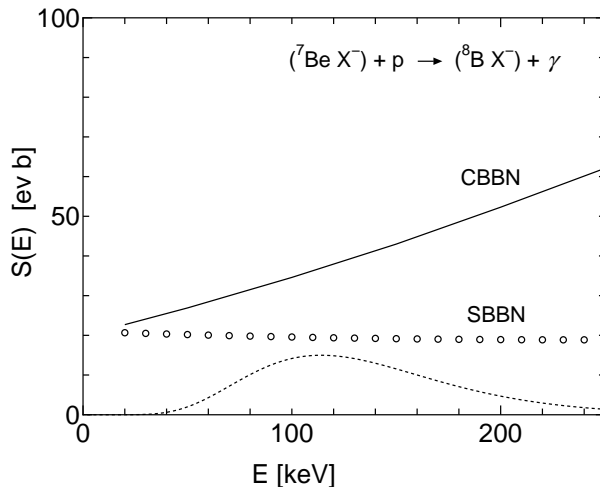


Fig. 8. The astrophysical S -factor (solid line) of the *nonresonant* radiative capture CBBN reaction (3.2) obtained by the three-body calculation. The observed S -factor of the SBBN partner reaction (3.24) is shown by open circles.¹⁸⁾ The dotted curve illustrates the Gamow peak (in arbitrary units) for $T_9 = 0.3$ ($kT = 35$ keV) with the maximum at $E_0 = 114$ keV.

The enhancement ratio CBBN/SBBN of the S -factor is only 1 – 2 in the Gamow peak region for the nonresonant radiative capture processes (3.2) and (3.24). However, in the work of Bird *et al.*,⁶⁾ this ratio is estimated to be as large as ~ 700 . The origin of this enormous overestimation is the crude assumption employed in their model. Namely, they assumed that the magnitude of the three-body E1 matrix

element in Eq. (3·23) is the same as that of the two-body E1 matrix element in SBBN. This is an incorrect assumption because, in the SBBN matrix element, the dominant contribution comes from the asymptotic tail region of the distance between ${}^7\text{Be}$ and the proton (along \mathbf{r}_2) in the loosely bound ground state of ${}^8\text{B}$, but, in the CBBN matrix element, the contribution is heavily suppressed by the presence of X^- as follows: (i) in the $({}^7\text{Be}X^-)_{1s}$ state of the initial channel, the distance between ${}^7\text{Be}$ and X^- along \mathbf{r}_1 is short (the rms radius is ~ 3.5 fm), (ii) in the final state $\Psi_{00}(E)$, the distance between ${}^8\text{B}$ and X^- along \mathbf{R}_2 is also short (the rms radius is ~ 3 fm), and thus (iii) these strongly confine the possible ${}^7\text{Be}-p$ distance along \mathbf{r}_2 that is effective in the three-body E1 matrix element. Therefore, the contribution from the asymptotic region along \mathbf{r}_2 is heavily suppressed. The CBBN/SBBN ratio of the S -factor becomes larger in the scaling model of Ref. 6) as the binding energy of $({}^8\text{B}X^-)$ increases, but, at the same time, the wave function of $({}^8\text{B}X^-)$ shrinks and therefore the three-body E1 matrix element becomes smaller. This consideration of this mechanism was missing in the simple model of Ref. 6) for the nonresonant radiative capture reaction.

The fact that the CBBN and SBBN S -factors have similar magnitudes, within factor nearly 2, in the Gamow peak region in Fig. 8 suggests an approximate model for the cross section $\sigma_{\text{cap}}^{(\text{E1})}(E)$ of the CBBN reaction. The cross section may roughly be derived from (2·21) by employing the observed S -factor of the SBBN-reaction and the Coulomb barrier penetration factor of the CBBN channel. Here, the SBBN *partner* reaction is defined as the reaction that is given by simply removing X^- from a CBBN reaction*). This approximate model will be further examined in the next section for complicated CBBN three-body breakup reactions.

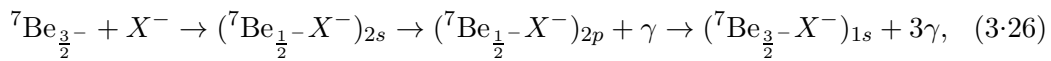
In Fig. 8, since the energy dependence of $S(E)$ may be approximated by (2·27) with $S(0) = 20 \times 10^{-3}$ keV b and $\alpha = 0.15 \times 10^{-3}$ b, the reaction rate is written as

$$N_A \langle \sigma v \rangle = 2.3 \times 10^5 T_9^{-\frac{2}{3}} \exp(-8.83 T_9^{-\frac{1}{3}}) (1 + 1.9 T_9^{\frac{2}{3}} + 0.54 T_9) \text{ cm}^3 \text{ s}^{-1} \text{ mol}^{-1}, \quad (3\cdot25)$$

for $T_9 \lesssim 0.5$. Since this rate is 4 orders of magnitude smaller than that of the resonant reaction (3·1) at $T_9 = 0.3 - 0.5$, the nonresonant radiative capture reaction (3·2) will play a very minor role in the BBN network calculation.

3.6. Comment on resonant recombination between ${}^7\text{Be}$ and X^-

The radiative capture processes (3·1) and (3·2) are preceded by the recombination of ${}^7\text{Be}$ and X^- to form $({}^7\text{Be}X^-)$. Bird *et al.*⁶⁾ calculated the reaction rates of the resonant and nonresonant processes of the recombination. We here make an important comment on a part of their calculation. In addition to the normal recombination processes (2·7) and (2·8) in Ref. 6), they specially considered another resonant recombination process, (2·12) in Ref. 6),



*) For instance, the reaction $\alpha + d \rightarrow {}^6\text{Li} + \gamma$ is not the SBBN partner of $(\alpha X^-) + d \rightarrow {}^6\text{Li} + X^-$ but that of $(\alpha X^-) + d \rightarrow ({}^6\text{Li}X^-) + \gamma$. There is no SBBNpartner of $(\alpha X^-) + d \rightarrow {}^6\text{Li} + X^-$.

where ${}^7\text{Be}_{\frac{3}{2}-}$ and ${}^7\text{Be}_{\frac{1}{2}-}$ are the ground state and first excited state at $E_x = 0.429$ MeV, respectively. Their calculated energy of the intermediate state $({}^7\text{Be}_{\frac{1}{2}-}X^-)_{2s}$ with $m_X \rightarrow \infty$ is 49 keV *below* the ${}^7\text{Be}_{\frac{3}{2}-} + X^-$ threshold, which means that the intermediate state cannot be a resonance in (3·26). Bird *et al.*, however, artificially pushed the state upward to a resonant energy of +10 keV above the threshold and derived a large recombination rate, Eq. (2·13) of Ref. 6). Their reason for doing this was that they expected ‘a sizable nuclear uncertainty’ such as a correction for the finite mass of X^- , a larger charge radius of the excited state and a correction for nuclear polarizability. The contribution of the ‘resonant’ $({}^7\text{Be}_{\frac{1}{2}-}X^-)_{2s}$ state is then capable of enhancing the recombination rate by a factor of a few. Bird *et al.* reported two types of results, *with* and *without* the $({}^7\text{Be}_{\frac{1}{2}-}X^-)_{2s}$ contribution, when they discussed the abundance of ${}^7\text{Li}$ - ${}^7\text{Be}$ and the lifetime and abundance of X^- particles.

To completely remove the above ‘nuclear uncertainty’ from the model, we perform an $\alpha + {}^3\text{He} + X^-$ three-body calculation of the energy of $({}^7\text{Be}_{\frac{1}{2}-}X^-)_{2s}$. The three-body Hamiltonian is the same as that used in §2, where we investigated the reaction $(\alpha X^-) + {}^3\text{He} \rightarrow {}^7\text{Be} + X^-$, but here we take into account the spins of ${}^3\text{He}$ and ${}^7\text{Be}$ using a spin dependent α - ${}^3\text{He}$ potential to reproduce the energies of ${}^7\text{Be}_{\frac{3}{2}-}$ and ${}^7\text{Be}_{\frac{1}{2}-}$. We find that the rms charge radius differs by only 0.05 fm between ${}^7\text{Be}_{\frac{3}{2}-}$ and ${}^7\text{Be}_{\frac{1}{2}-}$. According to the three-body calculation the energy of $({}^7\text{Be}_{\frac{1}{2}-}X^-)_{2s}$ is -41 keV for $m_X \rightarrow \infty$, -20 keV for $m_X = 100$ GeV and -2 keV for $m_X = 50$ GeV with respect to the ${}^7\text{Be}_{\frac{3}{2}-} + X^-$ threshold. Therefore, we conclude that the $({}^7\text{Be}_{\frac{1}{2}-}X^-)_{2s}$ state never becomes a resonance in the process of (3·26). In Ref. 6), two types of calculations of the element abundance *with* and *without* the $({}^7\text{Be}_{\frac{1}{2}-}X^-)_{2s}$ resonance are reported, but the case *with* the resonance is not acceptable.

The application of the $\alpha + {}^3\text{He} + X^-$ three-body calculation to the full recombination processes of ${}^7\text{Be}$ and X^- will be one of our future subjects of study since the transition between the ${}^7\text{Be}_{\frac{3}{2}-}$ and ${}^7\text{Be}_{\frac{1}{2}-}$ states due to X^- is an important factor in the recombination and can be unambiguously treated using the three-body model.

§4. X^- -catalyzed three-body breakup reactions

The most effective reactions for destroying ${}^6\text{Li}$ and ${}^7\text{Li}$ in SBBN are

$${}^6\text{Li} + p \rightarrow \alpha + {}^3\text{He} + 4.02 \text{ MeV} , \quad (4.1)$$

$${}^7\text{Li} + p \rightarrow \alpha + \alpha + 17.35 \text{ MeV} , \quad (4.2)$$

which have large S -factors ($S(0) \sim 3$ MeV b and ~ 0.06 MeV b, respectively¹⁸⁾). Therefore, the corresponding CBBN three-body breakup reactions,

$$({}^6\text{Li}X^-) + p \rightarrow \alpha + {}^3\text{He} + X^- + 3.22 \text{ MeV} , \quad (4.3)$$

$$({}^7\text{Li}X^-) + p \rightarrow \alpha + \alpha + X^- + 16.47 \text{ MeV} , \quad (4.4)$$

should be taken into account in BBN calculations^{*)}. However, the explicit calculation of these CBBN processes is tedious and difficult because (i) the exit channel is that of a three-body breakup, (ii) at least a four-body model, in which ${}^6\text{Li}$ (${}^7\text{Li}$) is composed of $d + \alpha$ ($t + \alpha$), is needed, (iii) $d(t)$ in ${}^6\text{Li}$ (${}^7\text{Li}$) must be picked up by the incoming proton to form ${}^3\text{He}$ (α) and (iv) it is tedious to reasonably determine all the three spin-dependent nuclear interactions appearing in the four-body model. Instead, a naive approximation often taken in BBN network calculations, for instance, in Refs. 4) and 12), is that the cross section of the CBBN reaction (4.3), and similarly that of (4.4), may be given by a product of the observed S -factor of the SBBN partner reaction (4.1) and the CBBN Coulomb barrier penetration factor, in which the charge of the target is reduced by one unit owing to the presence of X^- .

In this section, we propose a more sophisticated and phenomenologically reasonable three-body model to implement the information of the SBBN cross section into the CBBN calculation instead of carrying out an explicit calculation of (4.3) and (4.4). Firstly, we calculate the SBBN reactions (4.1) and (4.2). We do not explicitly treat the channel coupling between the entrance and exit channels. Instead, we employ only the entrance channel, say $(AX^-) + a$, and introduce a complex potential $V_{A-a}(r)$ between the particles A and a (here, $A = {}^6,7\text{Li}$ and $a = p$):

$$V_{A-a}(r) = V_{A-a}^{\text{(real)}}(r) + iV_{A-a}^{\text{(imag)}}(r) \quad (4.5)$$

as seen in nuclear optical model potentials. In this case, the absorption cross section in the elastic $A + a$ scattering is equivalent to the reaction cross section because there are no open channel other than the entrance and exit channels of (4.1) and (4.2). We determine the potential $V_{A-a}(r)$ so as to reproduce the observed SBBN cross section (S -factor).

Secondly, we incorporate this potential $V_{A-a}(r)$ into the three-body Hamiltonian (2.9) of the $A + a + X^-$ system and solve the elastic scattering between (AX^-) and a , namely the elastic $({}^6,7\text{Li}X^-) + p$ scattering. We consider that the absorption cross section obtained in this scattering calculation provides the cross section of the CBBN reaction^{**)}.

The wave function is written similarly to (2.12) but without the exit channel as

$$\Psi_{JM} = \phi_{00}^{(1)}(\mathbf{r}_1) \chi_{JM}^{(1)}(\mathbf{R}_1) + \Psi_{JM}^{\text{(closed)}}, \quad (4.6)$$

where $\phi_{00}^{(1)}(\mathbf{r}_1)$ represents the $1s$ wave function of $({}^6,7\text{Li}X^-)$ and $\chi_{JM}^{(1)}(\mathbf{R}_1)$ for the $({}^6,7\text{Li}X^-) + p$ scattering wave. The scattering boundary condition imposed on $\chi_{JM}^{(1)}(\mathbf{R}_1) (\equiv \chi_J^{(1)}(R_1) Y_{JM}(\hat{\mathbf{R}}_1))$ is given by

$$\lim_{R_1 \rightarrow \infty} R_1 \chi_J^{(1)}(R_1) = u_J^{(-)}(k_1, R_1) - S_{1 \rightarrow 1}^J u_J^{(+)}(k_1, R_1). \quad (4.7)$$

^{*)} Since the kinetic energy of the exit channel is large, the formation of the bound states ${}^7\text{Be}$, ${}^8\text{Be}$, (αX^-) and $({}^3\text{He}X^-)$ in (4.3) and (4.4) is not important and is not explicitly considered there.

^{**)} More precisely, this absorption cross section, for instance, in the case of $({}^6\text{Li}X^-) + p$ scattering, includes transitions to the $(\alpha X^-) + {}^3\text{He}$, $({}^3\text{He}X^-) + \alpha$ and ${}^7\text{Be} + X^-$ channels, which are possible in the presence of the X^- particle, but are of minor importance owing to the much smaller phase space than that in the three-body breakup channel.

Similarly to in the previous sections, the second term of (4.6), $\Psi_{JM}^{(\text{closed})}$, represents all the asymptotically vanishing three-body amplitudes that are not included in the first scattering term, and is expanded in terms of the eigenfunctions of the Hamiltonian (without the imaginary part of (4.5)) as

$$\Psi_{JM}^{(\text{closed})} = \sum_{\nu=1}^{\nu_{\text{max}}} b_{J\nu} \Phi_{JM,\nu}. \quad (4.8)$$

Using $S_{1 \rightarrow 1}^J$ in (4.7), we derive the reaction cross section as

$$\sigma_{\text{reac}} = \frac{\pi}{k_1^2} \sum_{J=0}^{\infty} (2J+1) (1 - |S_{1 \rightarrow 1}^J|^2). \quad (4.9)$$

This reaction (absorption) cross section can be expressed alternatively as

$$\sigma_{\text{reac}} = \frac{-2}{\hbar v_1} \langle \Psi_{JM} | V_{A-a}^{(\text{imag})}(r_2) | \Psi_{JM} \rangle. \quad (4.10)$$

These two types of σ_{reac} utilize information from different parts of the three-body wave function, namely, the information from the asymptotic part along \mathbf{R}_1 in the former expression and that from the internal part along \mathbf{r}_2 in the latter. Therefore, it is difficult to demonstrate the agreement between the two types of σ_{reac} . We obtained a precise agreement between their numbers to four significant figures, which demonstrates the high accuracy of our three-body calculation.

4.1. Nuclear complex potential and Coulomb potential

We construct the complex potential^{*)} (4.5) between ${}^6, {}^7\text{Li}$ and p so as to reproduce the observed low-energy S -factors of (4.1) and (4.2) (the adopted values in Ref. 18)). The shape of the potential is assumed as

$$V^{(\text{real})}(r) = V_0 [1 + \exp\{(r - R_0)/a_0\}]^{-1} + V_{\text{Li-}p}^{\text{C}}(r), \quad (4.11)$$

$$V^{(\text{imag})}(r) = W_0 [1 + \exp\{(r - R_I)/a_I\}]^{-1}. \quad (4.12)$$

The Coulomb potential $V_{\text{Li-}p}^{\text{C}}(r)$ is derived by assuming a Gaussian charge distribution for ${}^6\text{Li}$ (${}^7\text{Li}$) that reproduces the observed rms charge radius 2.54 fm (2.43 fm).²⁸⁾ The energies of (${}^6\text{Li}X^-$) and (${}^7\text{Li}X^-$) are -0.773 and -0.854 MeV, respectively, and the rms radii are 4.61 and 4.16 fm, respectively, when $m_X = 100$ GeV.

i) ${}^6\text{Li-}p$ potential

The potential parameters are chosen as follows: $V_0 = -59.5$ MeV, $R_0 = 2.5$ fm and $a = 0.6$ fm for the odd state and $V_0 = 400$ MeV, $R_0 = 1.5$ fm and $a = 0.2$ fm for the even state as well as $W_0 = -5.0$ MeV, $R_I = 2.5$ fm and $a_I = 0.6$ fm for both states. The repulsive potential for the even state is introduced as a substitute for the Pauli principle to exclude the s -state (the contribution from the d -state is negligible).

^{*)} We follow the same prescription as that employed in Ref. 40) to determine the nuclear fusion rate in a muonic molecule ($d\mu$) by using a complex potential between d and t .

ii) ${}^7\text{Li}$ - p potential

The potential parameters are chosen as follows: $V_0 = -77.2$ MeV, $R_0 = 2.5$ fm and $a = 0.6$ fm for the odd state, $V_0 = 400$ MeV, $R_0 = 1.5$ fm and $a = 0.2$ fm for the even state, and $W_0 = -1.1$ MeV, $R_I = 2.5$ fm and $a_I = 0.6$ fm for the odd state and $W_0 = 0$ for the even state. The reason for setting $W_0 = 0$ for the even state is that, in reaction (4.4), the odd angular momentum between the two α is prohibited, and therefore the even state of the ${}^7\text{Li}$ - p relative motion is forbidden (${}^7\text{Li}$ has odd parity). This explains why the observed S -factor of (4.4), $S(0) \sim 0.06$ MeV b, is much smaller than that of (4.3), $S(0) \sim 3$ MeV b.

4.2. Result for three-body breakup reactions

The calculated S -factors of the CBBN reactions (4.1) and (4.2) are shown in Figs. 9 and 10, respectively, together with those of the SBBN partner reactions.¹⁸⁾ It is interesting to note that the CBBN/SBBN ratio of the S -factor is nearly 0.6 – 1 in the Gamow peak region in both figures. Also, the ratio was nearly 1 – 2 in the previous case shown in Fig. 8. This suggests that the CBBN reaction cross section may be approximated, within an error of factor nearly 2, by a simple model in which the CBBN S -factor in (2.21) is replaced by the observed S -factor of the SBBN partner reaction but the Coulomb barrier penetration factor is kept the same as that in CBBN.

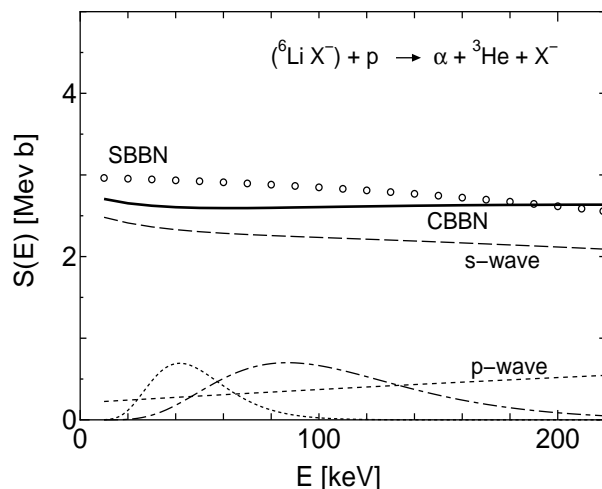


Fig. 9. The calculated S -factor for the CBBN reaction (4.1) (solid line). The s - and p -wave contributions are shown individually. The observed S -factor of the SBBN partner reaction (4.3) is given by open circles (the *adopted* values in Ref. 18)). The dotted curve illustrates the Gamow peak (in arbitrary units) for $T_9 = 0.1$ ($kT = 8.6$ keV) with the maximum at $E_0 = 42$ keV, and the dot-dashed curve is that for $T_9 = 0.3$ ($kT = 26$ keV) with $E_0 = 87$ keV.

This simple model may be used in BBN network calculations (and has already been employed in some calculations in the literature) when precise CBBN reaction rate is not available. However, the definition of the SBBN partner reaction should be applied strictly as discussed in §3.5.

The S -factor of the CBBN reaction (4.1) in Fig. 9 may be simulated using

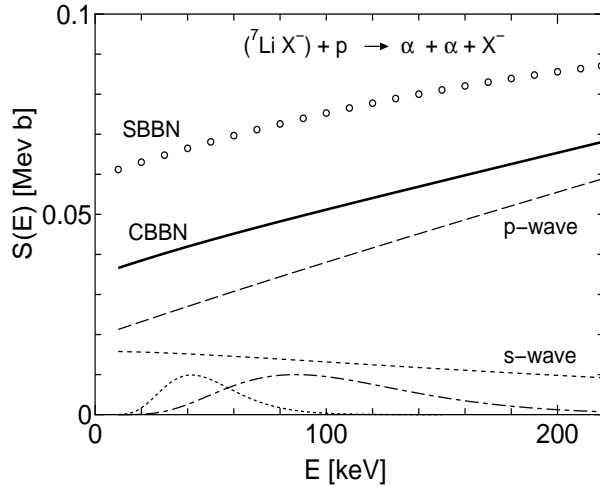


Fig. 10. The calculated S -factor for the CBBN reaction (4.2) (solid line). The s - and p -wave contributions are shown individually. The observed S -factor of the SBBN partner reaction (4.4) is given by open circles (the *adopted* values in Ref. 18). The dotted curve is the Gamow peak (in arbitrary units) for $T_9 = 0.1$ ($kT = 8.6$ keV) with the maximum $E_0 = 42$ keV, and the dot-dashed curve is that for $T_9 = 0.3$ ($kT = 26$ keV) with $E_0 = 87$ keV.

expression (2.27) with $S(E) \simeq 2.6 \times 10^3$ keV b. Using (2.28), the CBBN reaction rate for $T_9 \lesssim 0.5$ is then given as

$$N_A \langle \sigma v \rangle = 2.6 \times 10^{10} T_9^{-\frac{2}{3}} \exp(-6.74 T_9^{-\frac{1}{3}}) \text{ cm}^3 \text{ s}^{-1} \text{ mol}^{-1}. \quad (4.13)$$

In Fig. 10, which shows reaction (4.2), the energy dependence of $S(E)$ may be approximated by (2.27) with $S(0) = 36$ keV b and $\alpha = 0.15$ b, and therefore the reaction rate for $T_9 \lesssim 0.5$ is written as

$$N_A \langle \sigma v \rangle = 3.5 \times 10^8 T_9^{-\frac{2}{3}} \exp(-6.74 T_9^{-\frac{1}{3}}) (1 + 0.81 T_9^{\frac{2}{3}} + 0.30 T_9) \text{ cm}^3 \text{ s}^{-1} \text{ mol}^{-1}. \quad (4.14)$$

It will be interesting to see whether, in the BBN network calculation using the above reaction rates, the CBBN reactions (4.1) and (4.2) destroy significant amount of ${}^6,7\text{Li}$, since their SBBN partners (4.3) and (4.4) are the reactions that destroy ${}^6,7\text{Li}$ the most strongly in standard BBN.

§5. X^- -catalyzed charge-exchange reactions

When the cosmic temperature cools to $T_9 \sim 0.01$, the X^- particle begins to form the *neutral* bound state^{*)} (pX^-) if $\tau_X \gtrsim 10^6$ s; this is also true for (dX^-) and (tX^-), even though their fractions are very much smaller (cf., for example, Fig. 2 in Ref. 12)). Owing to the *lack* of a Coulomb barrier, the bound states are expected to interact strongly with other elements that have already been synthesized.

^{*)} The binding energy of (pX^-) is ~ 0.025 MeV and the rms radius is ~ 50 fm.

In this section, we perform a fully quantum three-body calculation of the following CBBN reactions that are induced by the neutral bound states (pX^-), (dX^-) and (tX^-):

a) Charge-exchange reactions,

$$(pX^-) + \alpha \rightarrow (\alpha X^-)_{3s,3p,3d} + p \quad (5.1)$$

$$(dX^-) + \alpha \rightarrow (\alpha X^-)_{2s,2p} + d \quad (5.2)$$

$$(tX^-) + \alpha \rightarrow (\alpha X^-)_{2s,2p} + t \quad (5.3)$$

b) Reactions that produce ${}^6,{}^7\text{Li}$,

$$(dX^-) + \alpha \rightarrow {}^6\text{Li} + X^- + 1.4 \text{ MeV} , \quad (5.4)$$

$$(tX^-) + \alpha \rightarrow {}^7\text{Li} + X^- + 2.4 \text{ MeV} , \quad (5.5)$$

c) Reactions that destroy ${}^6,{}^7\text{Li}$ and ${}^7\text{Be}$,

$$(pX^-) + {}^6\text{Li} \rightarrow \alpha + {}^3\text{He} + X^- + 4.0 \text{ MeV} , \quad (5.6)$$

$$(pX^-) + {}^7\text{Li} \rightarrow \alpha + \alpha + X^- + 17 \text{ MeV} , \quad (5.7)$$

$$(pX^-) + {}^7\text{Be} \rightarrow {}^8\text{B} + X^- + 0.11 \text{ MeV} . \quad (5.8)$$

In the charge-exchange reactions, the excited states of the (αX^-) atom with the principal quantum numbers $n = 3$ and 2 are respectively employed in (5.1) and (5.2)–(5.3). They have the minimum transferred energy among the energetically possible (αX^-) $_{nl}$ states.*)

Upon performing a DWBA calculation, Jedamzik^{9),10)} asserted that the cross sections of the CBBN reactions (5.6) and (5.8) that destroy ${}^6\text{Li}$ and ${}^7\text{Be}$, respectively, are so large that (pX^-) could induce a second round of BBN, say late-time BBN, capable of destroying most of the previously synthesized ${}^6\text{Li}$ and ${}^7\text{Be}$. However, since the strength of the nuclear interactions (on the order of ~ 10 MeV) that cause reactions (5.6) and (5.8) is much larger than the incident energy ($\lesssim 1$ keV), the Born approximation should not be applied to these low-energy nuclear reactions.

Since the neutral bound state in the entrance channel behaves like a neutron at a large distance with no Coulomb barrier, reactions (5.4)–(5.8) caused by the nuclear interaction are expected to have greatly enhanced cross sections even at low energies (< 1 keV). Therefore, the most interesting issue in this section is whether or not the charge-exchange reactions are so strong that they can intercept the reactions (5.4)–(5.8) that produce and destroy Li and Be.

Before performing a precise quantum three-body calculation, we make a simple consideration, following the semiclassical approach in Refs. 14) and 41), to compare the cross section of the *atomic* process (5.1) with that of the *nuclear* reactions (5.4)–(5.8). In an analogy to the charge-exchange reactions seen in atomic physics, such as the capture of a muon by a hydrogen atom⁴¹⁾

$$(pe^-)_{1s} + \mu^- \rightarrow (p\mu^-)_{nl} + e^- , \quad (n \sim 14) \quad (5.9)$$

*) The energies of the $1s$ state of (pX^-), (dX^-) and (tX^-) are -25 , -48 and -71 keV, respectively, whereas those of (αX^-) $_{nl}$ are -337 keV($1s$), -96 keV($2p$), -90 keV($2s$), -43 keV($3d$), -43 keV($3p$) and -41 keV($3s$).

we understand that, if the incident α particle in (5.1) enters inside the proton 1s orbit of (pX^-), the sum of the inner charges seen by the proton becomes positive ($+e$), and therefore the proton immediately escapes from the orbit and instead the α particle is trapped by X^- as long as the incident energy is not too high. In the limit of the semiclassical picture, the cross section of (5.1) is approximately πb^2 , where b is the rms radius of the (pX^-) atom ($b = 50.4$ fm). On the other hand, the cross section of the nuclear reaction is roughly πb_0^2 , where b_0 is the sum of the radius of the incoming nucleus and the nuclear interaction range ($b_0 \sim$ several fm). Therefore, the atomic cross section is roughly two orders of magnitude larger than the nuclear cross section. Actually, this picture is not fully applicable because the quantum effect is large for low-lying orbits with $n \leq 3$. However, we find that the following quantum three-body calculations give a roughly similar ratio of the two cross sections, although each shows a strong energy dependence contrary to the above simple consideration.

a) Charge-exchange reactions

The method of calculating the cross sections of the charge-exchange reactions (5.1)–(5.3) is almost the same as that using Eqs. (2.8)–(2.20). For instance, for the reaction (5.1), the entrance channel (pX^-) + α is considered using the Jacobi coordinate system with $c = 1$ in Fig. 1, whereas the exit channel (αX^-)_{nl} + p is considered using the system with $c = 3$. For the closed-channel amplitude $\Psi_{JM}^{(\text{closed})}$ in (2.14), we take the same method as that in §2.4. The Coulomb potentials are constructed by assuming Gaussian charge distributions of p, d, t and α , the same as in the previous sections. Nuclear interactions play a negligible role in these atomic processes.

b) Reactions that produce Li

The α -transfer reactions (5.4) and (5.5) have the same structure as (2.2) and (2.4), respectively. Therefore, the method for calculating the cross sections of the former reaction is the same as that in §2 except that the entrance channel here is described using the Jacobi coordinate system with $c = 3$ in Fig. 1.

c) Reactions that destroy Li and Be

The two reactions (5.6) and (5.7) have the same structure as (4.3) and (4.4), respectively. Thus, the method for calculating them is the same. The structure of reaction (5.8) is similar to that of (3.2), although ${}^8\text{B}$ and X^- are not in a bound state here but in a photonless scattering state. In (3.2), the transition from the entrance channel to the exit channel via the electromagnetic interaction was treated perturbatively, but reaction (5.8) is solved as a ${}^7\text{Be} + p + X^-$ three-body problem.

5.1. Results

The calculated cross sections $\sigma(E)$ of reactions (5.1)–(5.8) are listed in Table II for energies $E = 0.01, 0.1, 1$ and 10 keV ($T_9 \sim 0.0001, 0.001, 0.01$ and 0.1 , respectively). Since the Coulomb barrier penetration factor $\exp(-2\pi\eta(E))$ in (2.21) is unity here, the astrophysical S -factor is simply given by $S(E) = E\sigma(E)$.

The extreme enhancement of the cross sections of reactions (5.4)–(5.8) due to

the neutral bound states can be seen, for example, by the fact that the ${}^6\text{Li}$ production cross section of (5.4) at $E = 10$ keV is 6.4×10^{-1} b, whereas that of (2.2) with (αX^-) in the entrance channel is 3.9×10^{-6} b.⁵⁾ As can be seen in the usual *neutron*-induced low-energy reactions, the cross sections roughly follows the $1/v$ law at lower energies ($\lesssim 1$ keV) in Table II.

Table II. Calculated cross sections and reaction rates of the late-time BBN reactions induced by the neutral bound states. The rates (in units of $\text{cm}^3 \text{s}^{-1} \text{mol}^{-1}$) are applicable for $T_9 \lesssim 0.05$.

Reaction	cross section (b)				reaction rate
	0.01 keV	0.1keV	1 keV	10 keV	
a) charge-exchange reaction					
$(pX^-) + \alpha \rightarrow (\alpha X^-)_{3\ell} + p$	8.4×10^3	2.2×10^3	7.8×10^2	7.5×10^1	1.0×10^{10}
$(dX^-) + \alpha \rightarrow (\alpha X^-)_{2\ell} + d$	3.1×10^3	9.1×10^2	2.0×10^2	2.1×10^1	3.5×10^9
$(tX^-) + \alpha \rightarrow (\alpha X^-)_{2\ell} + t$	8.3×10^3	1.9×10^3	3.2×10^2	2.5×10^1	7.6×10^9
b) α -transfer reaction					
$(dX^-) + \alpha \rightarrow {}^6\text{Li} + X^-$	9.6×10^0	3.0×10^0	6.9×10^{-1}	6.4×10^{-1}	1.1×10^7
$(tX^-) + \alpha \rightarrow {}^7\text{Li} + X^-$	3.5×10^{-1}	1.1×10^{-1}	2.7×10^{-2}	3.0×10^{-2}	4.3×10^5
c) Li-Be destruction					
$(pX^-) + {}^6\text{Li} \rightarrow \alpha + {}^3\text{He} + X^-$	1.8×10^2	5.5×10^1	1.1×10^1	2.8×10^0	1.6×10^8
$(pX^-) + {}^7\text{Li} \rightarrow \alpha + \alpha + X^-$	3.8×10^0	1.7×10^0	7.7×10^{-1}	1.6×10^{-1}	5.5×10^6
$(pX^-) + {}^7\text{Be} \rightarrow {}^8\text{B} + X^-$	4.8×10^{-1}	3.2×10^0	5.3×10^{-1}	5.5×10^{-2}	5.2×10^6

The most important result in Table II is that the cross sections of the charge-exchange reactions are much larger than those of the nuclear reactions (5.4)–(5.8). Therefore, for the α -transfer reactions (5.4) and (5.5), the bound states (dX^-) and (tX^-) are mostly changed to (αX^-) before producing ${}^{6,7}\text{Li}$. For the Li-Be destruction reactions (5.6)–(5.8), we further note that the probability that (pX^-) comes in contact with ${}^{6,7}\text{Li}$ and ${}^7\text{Be}$ is more than several orders of magnitude smaller than that of it coming in contact with an α particle owing to the large difference in the element abundances, and that, even if (pX^-) did collide with an element A ($={}^{6,7}\text{Li}$ or ${}^7\text{Be}$), another atomic charge-exchange reaction,

$$(pX^-) + A \rightarrow (AX^-)_{nl} + p, \quad (A = {}^{6,7}\text{Li}, {}^7\text{Be}) \quad (5.10)$$

would immediately occur instead of reactions (5.6)–(5.8) since the cross section of (5.10) would be as large as that in (5.1), although it was not calculated here.

To conclude, the nuclear reactions (5.4)–(5.8) that produce and destroy Li and Be would negligibly change the element abundance in the late-time BBN owing to the strong interception by the charge-exchange reactions (5.1)–(5.3) and (5.10).

We derive the reaction rates of (5.1)–(5.8) for use in the network BBN calculation under the approximation that the cross sections in Table II may be roughly simulated in a simple form (the $1/v$ law)

$$\sigma(E) \approx C/\sqrt{E}. \quad (5.11)$$

An evident reduction of the cross section in Table II from (5.11) can be seen at $E \sim 10$ keV due to the structure of the neutral bound state and the decreased probability of the α particle being trapped by X^- , but this reduction is thought to have little effect on the element abundance^{*}). The use of this approximation in the calculation of the reaction rate (2.23) makes the result independent of the temperature T_9 .^{**}) The rate for $T_9 \lesssim 0.05$ is described as

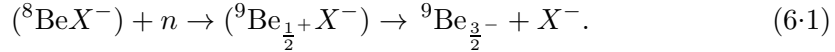
$$N_A \langle \sigma v \rangle = 2.6 \times 10^7 \sqrt{E_m/\mu} \sigma(E_m) \quad \text{cm}^3 \text{s}^{-1} \text{mol}^{-1}, \quad (5.12)$$

where the constant C is determined by matching (5.11) to $\sigma(E)$ in Table II at $E = E_m$. Here, E_m and $\sigma(E_m)$ are expressed in units of keV and b, respectively, and μ is the reduced mass of the entrance channel in units of amu. We then simply averaged the three rates determined at $E_m = 0.01, 0.1$ and 1 (keV).

The calculated reaction rates are listed in the last column of Table II. We consider that it is not necessary to simulate $\sigma(E)$ in a more sophisticated manner than (5.11), because it is clear from Table II and the above discussion that the late-time BBN does not affect the element abundances meaningfully^{***}). A similar conclusion on the effect of the late-time BBN was obtained in Ref. 14).

§6. X^- -catalyzed production of ${}^9\text{Be}$

The absence of stable isotopes with mass number 8 is a bottleneck for the production of ${}^9\text{Be}$ and heavier nuclei in standard BBN. In recent papers,^{13),14)} Pospelov and coworkers pointed out the possibility of the enormous enhancement of the reaction rate for the production of ${}^9\text{Be}$ by considering an X^- -catalyzed *resonant* neutron-capture process



They claimed that the primordial abundance of ${}^9\text{Be}$ imposes strong restrictions on the lifetime and abundance of X^- . Here, ${}^9\text{Be}_{\frac{3}{2}^-}$ is the ground state and ${}^9\text{Be}_{\frac{1}{2}^+}$ denotes the first excited state with spin $\frac{1}{2}^+$ at $E_x = 1.735 \pm 0.003$ MeV with the neutron decay width $\Gamma_n = 0.225 \pm 0.012$ MeV⁴³⁾ (or $E_x = 1.684 \pm 0.007$ MeV with $\Gamma_n = 0.225 \pm 0.012$ MeV⁴⁴⁾).

In this section, we make a critical comment on this work.^{13),14)} Their attention to reaction (6.1) is interesting, but there is a serious problem in their calculation.

^{*}) Also, the cross section at $E = 0.01$ keV in the bottom line of Table II is much smaller than that given by (5.11), but this is because the p -wave contribution is dominant in (5.8) and momentum matching becomes difficult at low energies when the proton is transferred to a definite bound state in the exit channel.

^{**}) Pospelov *et al.*¹⁴⁾ derived the rate as $\propto 1/\sqrt{T_9}$, but this is due to the fact that they did not calculate the energy dependence of the cross section and assumed it to be constant with respect to the energy. Their value at $T_9 = 0.01$ is of the same order of magnitude as ours for $(pX^-) + \alpha \rightarrow (\alpha X^-)_{\text{exc.}} + p$.

^{***}) According to a BBN network calculation by Kusakabe⁴²⁾ including the reaction rates in Table II, the abundances of the bound states (pX^-) , (dX^-) and (tX^-) at $T_9 \lesssim 0.05$ are greatly reduced by a factor of $\sim 10^5$ from those obtained without including the reaction rates.

They assumed that the rms charge radius of both ${}^8\text{B}$ and ${}^9\text{Be}$ was 2.50 fm. Since the observed charge radius of ${}^9\text{Be}_{\frac{3}{2}-}$ is 2.519 ± 0.012 fm,⁴⁴⁾ the assumed radius is acceptable for ${}^9\text{Be}_{\frac{3}{2}-}$. However, there is no reason to take a radius of 2.50 fm for ${}^8\text{Be}$, which is a resonance state at 0.092 MeV above the $\alpha + \alpha$ threshold. In principle, the radius of such a resonance state cannot be experimentally measured, and even theoretically, it is difficult to define the radius of the oscillating resonance wave function. Since the width of this resonance is, however, very small (5.57 eV), the wave function is heavily attenuated by the Coulomb barrier, followed by an asymptotically oscillating amplitude that is roughly three orders of magnitude smaller than that in the nuclear interaction region. Therefore, it is not meaningless to derive the rms radius by using the resonance wave function with the asymptotic part omitted, or by using the wave function obtained through the diagonalization of the Hamiltonian with appropriate L^2 -integrable basis functions; both methods result in almost the same radius as long as they give the same resonance energy.

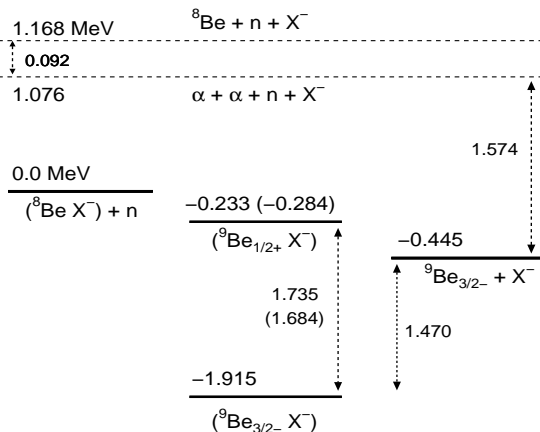


Fig. 11. Isobar diagram for the ${}^8\text{Be}+n+X^-$ system. This is to be compared with Fig. 1 of Ref. 13); here the same model as that in Ref. 13) is employed but the rms charge radius of ${}^8\text{Be}$ is changed to an appropriate value from the too small radius used in Ref. 13)(see text). It is demonstrated that the $({}^9\text{Be}_{\frac{1}{2}+}X^-)$ state becomes *below* the $({}^8\text{Be}X^-)+n$ threshold contrary to Ref. 13).

A microscopic $\alpha+\alpha$ model calculation using the resonating group method (RGM) by Arai *et al.*⁴⁵⁾ gives 3.16 fm for the rms charge radius of ${}^8\text{Be}$ but the resonance is 0.022 MeV above the $\alpha + \alpha$ threshold. A similar calculation with the orthogonality-condition model (OCM)²⁹⁾ by the present authors and their coworkers⁴⁶⁾ gives a radius of 3.39 fm when the $\alpha + \alpha$ resonance is at the observed position of 0.092 MeV. Since the latter model gives 3.20 fm when the resonance energy is tuned to the same value (0.022 MeV) as that in the former RGM calculation, we here employ an rms charge radius of ${}^8\text{Be}$ of 3.39 fm.

We now repeat the same analysis as that in Refs. 13) and 14), using the same

model but with charge radii of 3.39 and 2.52 fm for ${}^8\text{Be}$ and ${}^9\text{Be}$, respectively. Here, $m_X \rightarrow \infty$ is taken similarly to Ref. 13). As illustrated in Fig. 11, the binding energies of $({}^8\text{Be}X^-)$ and $({}^9\text{Be}_{\frac{3}{2}-}X^-)$ are respectively 1.168 and 1.470 MeV with respect to the ${}^8\text{Be} + X^-$ threshold and ${}^9\text{Be}_{\frac{3}{2}-} + X^-$ threshold that is located 1.574 MeV below the $\alpha + \alpha + n + X^-$ threshold. If we assume, similarly to in Ref. 13), that ${}^9\text{Be}_{\frac{1}{2}+}$ has the same charge radius as ${}^9\text{Be}_{\frac{3}{2}-}$, then the $({}^9\text{Be}_{\frac{1}{2}+}X^-)$ state is 1.735 MeV⁴³⁾ (or 1.684 MeV⁴⁴⁾) above $({}^9\text{Be}_{\frac{3}{2}-}X^-)$. As a result, we find that $({}^9\text{Be}_{\frac{1}{2}+}X^-)$ is not a resonance state but a bound state located 0.233 MeV (0.284 MeV) below the $({}^8\text{Be}X^-) + n$ threshold with no neutron decay width (although the state has a small width allowing decay to the ${}^9\text{Be}_{\frac{3}{2}-} + X^-$ channel). Those level energies depend on the shape of the charge distributions of ${}^8\text{Be}$ and ${}^9\text{Be}$, but the effect on the energy *difference* between the $({}^9\text{Be}_{\frac{1}{2}+}X^-)$ state and the $({}^8\text{Be}X^-) + n$ threshold is very small; for example, the difference changes by only 0.005 MeV if the charge distribution is artificially changed from Gaussian to square in both the nuclei. We thus conclude that the resonant neutron-capture process (6.1) is not realized as long as the model in Ref. 13) is employed.

Another problem in the analysis in Refs. 13) and 14) is that the charge radius of the excited resonance state ${}^9\text{Be}_{\frac{1}{2}+}$ is assumed to be the same as that of the ground state of ${}^9\text{Be}_{\frac{3}{2}-}$. An $\alpha + \alpha + n$ three-body RGM calculation by Arai *et al.*⁴⁵⁾ gave 2.88 fm for the rms charge radius of ${}^9\text{Be}_{\frac{1}{2}+}$. The calculated energy is ~ 0.4 MeV above the $\alpha + \alpha + n$ threshold while the observed value is 0.161 MeV⁴³⁾ (0.110 MeV⁴⁴⁾). The calculated neutron-decay width of ~ 0.2 MeV almost reproduces the experimental value. According to Arai *et al.*,⁴⁵⁾ an artificial change of the resonance position, even down to slightly below the $\alpha + \alpha + n$ threshold (by tuning a part of the interaction), has little effect on the charge radius of ${}^9\text{Be}_{\frac{1}{2}+}$; this is because the change in the wave function is dominantly seen in the resonating valence neutron and little change is seen in the α clusters. If we employ the charge radius of 2.88 fm for ${}^9\text{Be}_{\frac{1}{2}+}$, the energy -0.233 MeV (-0.284 MeV) of $({}^9\text{Be}_{\frac{1}{2}+}X^-)$ shown in Fig. 11 must be replaced by -0.116 MeV (-0.167 MeV). Therefore, the consideration of the differences in the rms charge radii among ${}^8\text{Be}$, ${}^9\text{Be}_{\frac{3}{2}-}$ and ${}^9\text{Be}_{\frac{1}{2}+}$ still causes the $({}^9\text{Be}_{\frac{1}{2}+}X^-)$ state to lie below the $\alpha + \alpha + n$ threshold.

In the above discussions on (6.1), it is still necessary to consider the change in structure of the *loosely coupled* systems ${}^8\text{Be}$ and ${}^9\text{Be}_{\frac{1}{2}+}$ induced by the addition of X^- to them. The dynamics can only be studied by employing an $\alpha + \alpha + n + X^-$ four-body model.*) Use of this model will also make it possible to exactly calculate the $({}^8\text{Be}X^-)$ formation processes $\alpha + X^- \rightarrow (\alpha X^-) + \gamma$, $(\alpha X^-) + \alpha \rightarrow ({}^8\text{Be}X^-) + \gamma$

*) This type of structure change by the injection of an impurity particle into loosely coupled nuclear states has well been studied in light hypernuclei by the present authors and their coworkers⁴⁶⁾⁻⁴⁹⁾ using three- and four-body models.

and the resonant (nonresonant) ${}^9\text{Be}_{\frac{3}{2}}^-$ formation process (6.1). This study based on the four-body model is beyond the scope of the present paper, but such a study is in progress and will be presented in the near future.

§7. Summary

(1) Using a fully quantum three-body method developed by the authors,¹⁷⁾ we have calculated the cross sections of various types of big-bang nucleosynthesis (BBN) reactions that are catalyzed by a hypothetical long-lived negatively charged, massive leptonic particle (called X^-) such as the supersymmetric (SUSY) particle *stau*. We also provided their reaction rates for use in the BBN network calculation. The rates are summarized in Table III and in the last column of Table II (the late-time BBN reactions for $T_9 \lesssim 0.05$).

(2) In the catalyzed BBN (CBBN) reactions, the strength of the nuclear interaction (on the order of 10 MeV), which causes the transition between the entrance and exit channels, is very much larger than the incident energy ($\lesssim 200$ keV), and therefore the coupling between the two channels is sufficiently strong to induce multistep transitions between the channels. Therefore, any calculation method that does not take into account the above property of the interaction is not suitable for application to the reactions. Also, for the charge-exchange reactions (5.1)–(5.3), a fully quantum, nonperturbative treatment is highly desirable since the α -particle is transferred to low-lying states with the principal quantum number $n = 2 - 3$. We have shown that our three-body calculation method¹⁷⁾ satisfies the above requirements and is useful for the study of all the reactions.

Table III. Summary of the calculated reaction rates of CBBN reactions obtained by the three-body calculation. a) - c) are for $T_9 \lesssim 0.2$ and d) - g) are for $T_9 \lesssim 0.5$.

Reaction	Reaction rate ($\text{cm}^3 \text{s}^{-1} \text{mol}^{-1}$)	
<i>nonresonant reaction</i>		
a) $(\alpha X^-) + d \rightarrow {}^6\text{Li} + X^-$	$2.78 \times 10^8 T_9^{-\frac{2}{3}} \exp(-5.33 T_9^{-\frac{1}{3}})$	$(1 - 0.62 T_9^{\frac{2}{3}} - 0.29 T_9)$
b) $(\alpha X^-) + t \rightarrow {}^7\text{Li} + X^-$	$1.4 \times 10^7 T_9^{-\frac{2}{3}} \exp(-6.08 T_9^{-\frac{1}{3}})$	$(1 + 1.3 T_9^{\frac{2}{3}} + 0.55 T_9)$
c) $(\alpha X^-) + {}^3\text{He} \rightarrow {}^7\text{Be} + X^-$	$9.4 \times 10^7 T_9^{-\frac{2}{3}} \exp(-9.66 T_9^{-\frac{1}{3}})$	$(1 + 0.20 T_9^{\frac{2}{3}} + 0.05 T_9)$
d) $({}^6\text{Li} X^-) + p \rightarrow \alpha + {}^3\text{He} + X^-$	$2.6 \times 10^{10} T_9^{-\frac{2}{3}} \exp(-6.74 T_9^{-\frac{1}{3}})$	
e) $({}^7\text{Li} X^-) + p \rightarrow \alpha + \alpha + X^-$	$3.5 \times 10^8 T_9^{-\frac{2}{3}} \exp(-6.74 T_9^{-\frac{1}{3}})$	$(1 + 0.81 T_9^{\frac{2}{3}} + 0.30 T_9)$
f) $({}^7\text{Be} X^-) + p \rightarrow ({}^8\text{B} X^-) + \gamma$	$2.3 \times 10^5 T_9^{-\frac{2}{3}} \exp(-8.83 T_9^{-\frac{1}{3}})$	$(1 + 1.9 T_9^{\frac{2}{3}} + 0.54 T_9)$
<i>resonant reaction</i>		
g) $({}^7\text{Be} X^-) + p \rightarrow ({}^8\text{B} X^-)_{2p}^{\text{res}}$	$1.37 \times 10^6 T_9^{-\frac{3}{2}} \exp(-2.28 T_9^{-1})$	$m_X = 50\text{GeV}$
$\rightarrow ({}^8\text{B} X^-) + \gamma$	$1.44 \times 10^6 T_9^{-\frac{3}{2}} \exp(-2.15 T_9^{-1})$	$m_X = 100\text{GeV}$
	$1.48 \times 10^6 T_9^{-\frac{3}{2}} \exp(-2.04 T_9^{-1})$	$m_X = 500\text{GeV}$
	$1.51 \times 10^6 T_9^{-\frac{3}{2}} \exp(-2.01 T_9^{-1})$	$m_X \rightarrow \infty$

(3) In the typical photonless CBBN reactions a)–c) in Table III, the calculated S -factors have similar orders of magnitude to those of the typical nonresonant photonless reactions in standard BBN (SBBN). As was first pointed out by Pospelov¹⁾ and then confirmed by Hamaguchi *et al.*,⁵⁾ the S -factor of CBBN reaction a) that produces ${}^6\text{Li}$ is many orders of magnitude larger than that of the radiative capture $\alpha + d \rightarrow {}^6\text{Li} + \gamma$ in SBBN. This imposes strong restrictions on the lifetime and abundance of X^- . However, this large enhancement is simply because this SBBN reaction is heavily E1-hindered. On the other hand, the S -factors of CBBN reactions b) and c) are found to be only ~ 30 times larger than those of the strong E1 radiative capture SBBN reactions $\alpha + t({}^3\text{He}) \rightarrow {}^7\text{Li}({}^7\text{Be}) + \gamma$. Therefore, reactions b) and c) do not seem to change the abundances of ${}^7\text{Li}$ - ${}^7\text{Be}$ meaningfully.

(4) The resonant radiative capture CBBN reaction, g) in Table III (cf. Fig. 5), was proposed by Bird *et al.*⁶⁾ as a possible solution to the overproduction of ${}^7\text{Li}$ - ${}^7\text{Be}$. We have examined their model and result using a ${}^7\text{Be} + p + X^-$ three-body model, which makes it possible to calculate all the steps in the reaction. We have shown that both the very loosely coupled ${}^7\text{Be} + p$ structure of ${}^8\text{B}$ and the strongly spin-dependent ${}^7\text{Be}_{\frac{3}{2}-} - p$ interaction contribute largely to the energy of the resonance $({}^8\text{B}X^-)_{2p}^{\text{res}}$. However, the effects work oppositely, almost cancelling each other, and therefore the reaction rate obtained by the simple model⁶⁾ (assuming a Gaussian charge distribution of ${}^8\text{B}$) is by chance close to ours. The reaction rate is sensitive to m_X ; the rate with $m_X = 100$ GeV is 60% of that with $m_X \rightarrow \infty$ at $T_9 = 0.3$.

Regarding the recombination process that forms $({}^7\text{Be}_{\frac{3}{2}-}X^-)$ starting from ${}^7\text{Be}_{\frac{3}{2}-}$ and a proton, we pointed out in §3.6 that the calculation⁶⁾ by Bird *et al.* of the energy of the ‘resonance’ state $({}^7\text{Be}_{\frac{1}{2}-}X^-)_{2s}$ is erroneous owing to the lack of consideration of the nuclear structure of ${}^7\text{Be}_{\frac{3}{2}-}$ and ${}^7\text{Be}_{\frac{1}{2}-}$; the $\alpha + {}^3\text{He} + X^-$ three-body calculation clarified that the $({}^7\text{Be}_{\frac{1}{2}-}X^-)_{2s}$ state cannot be a resonance but must be a bound state below the ${}^7\text{Be}_{\frac{3}{2}-} + X^-$ threshold. In Ref. 6) two types of results were reported on the abundance of ${}^7\text{Li}$ - ${}^7\text{Be}$ calculated *with* and *without* the $({}^7\text{Be}_{\frac{1}{2}-}X^-)_{2s}$ resonance, but the case *with* the resonance is not acceptable.

(5) We have performed fully quantum mechanical study on the late-time BBN reactions (5.1)–(5.8), which take place at $T_9 \lesssim 0.01$ between the neutral bound states, (pX^-) , (dX^-) and (tX^-) , and light nuclei. The atomic charge-exchange reactions (5.1)–(5.3) are so dominant that they immediately intercept the nuclear reactions (5.4)–(5.8). Therefore, we conclude that change of element abundances due to the late-time BBN reactions is negligible.

(6) We have examined the ‘resonant’ neutron-capture CBBN process (6.1) for producing ${}^9\text{Be}$ proposed by Pospelov and coworkers.^{13),14)} They claimed that the resulting increased output of ${}^9\text{Be}$ strongly constrains the abundance and lifetime of X^- . However, we found that, as long as the same model as that in Ref. 13) is employed but with an appropriate charge radius of ${}^8\text{Be}$ (a too small value of the

radius was used in Ref. 13)), the intermediate state (${}^9\text{Be}_{\frac{1}{2}^+}X^-$) appears *below* the (${}^8\text{Be}X^-$) + n threshold, thus giving no resonant mechanism. The model is, however, too simple to account for the change in the structure of the *loosely coupled* (resonant) systems ${}^8\text{Be}$ and ${}^9\text{Be}_{\frac{1}{2}^+}$ due to the injection of the X^- particle into them. Therefore, an extended four-body calculation based on an $\alpha + \alpha + n + X^-$ model is underway to examine (6.1) much more seriously.

(7) Finally, we expect that the application of the presently obtained reaction rates to the BBN network calculation will help solve the ${}^6\text{Li}$ - ${}^7\text{Li}$ problem and simultaneously impose restrictions on the primordial abundance and lifetime of the X^- particle.

Acknowledgements

The authors would like to acknowledge helpful discussions with M. Kusakabe on the BBN network calculation and with K. Arai on the structure of ${}^8\text{Be}$ and ${}^9\text{Be}$. They are also grateful to K. Hamaguchi, T. Hatsuda and T. T. Yanagida for valuable discussions on stau-catalyzed BBN reactions. This work was supported in part by a Grant-in-Aid for Scientific Research from the Ministry of Education, Culture, Sports, Science and Technology of Japan. The numerical calculations were performed on a HITACHI SR11000 at KEK and a FUJITSU PRIMEQUEST 580 at Kyushu University.

References

- 1) M. Pospelov, Phys. Rev. Lett. **98** (2007), 231301, hep-ph/0605215.
- 2) K. Kohri and F. Takayama, Phys. Rev. D **76** (2007), 063507, hep-ph/0605243.
- 3) M. Kaplinghat and A. Rajaraman, Phys. Rev. D **74** (2006), 103004, astro-ph/0606209.
- 4) R. H. Cyburt, J. Ellis, B. D. Fields, K. A. Olive and V. C. Spanos, J. Cosmol. Astropart. Phys. **11** (2006), 014, astro-ph/0608562.
- 5) K. Hamaguchi, T. Hatsuda, M. Kamimura, Y. Kino and T. T. Yanagida, Phys. Lett. B **650** (2007), 268, hep-ph/0702274.
- 6) C. Bird, K. Koopmans and M. Pospelov, Phys. Rev. D **78** (2008), 083010, hep-ph/0703096v3.
- 7) M. Kawasaki, K. Kohri and T. Moroi, Phys. Lett. B **649** (2007), 436, hep-ph/0703122.
- 8) T. Jittoh, K. Kohri, K. Koike, J. Sato, T. Shimomura and M. Yamanaka, Phys. Rev. D **76** (2007), 125023, hep-ph/0704.2914.
- 9) K. Jedamzik, Phys. Rev. D **77** (2008), 063524, astro-ph/0707.2070.
- 10) K. Jedamzik, J. Cosmol. Astropart. Phys. **03** (2008), 008, astro-ph/0710.5153.
- 11) M. Kusakabe, T. Kajino, R. N. Boyd, T. Yoshida and G. Mathews, Phys. Rev. D **76** (2007), 121302, astro-ph/0711.3854.
- 12) M. Kusakabe, T. Kajino, R. N. Boyd, T. Yoshida and G. J. Mathews, Astrophys. J. **680** (2008), 846, astro-ph/0711.3858.
- 13) M. Pospelov, hep-ph/0712.0647.
- 14) M. Pospelov, J. Pradler and F. D. Steffen, J. Cosmol. Astropart. Phys. **11** (2008), 026, hep-ph/0807.4287.
- 15) For example, J.L. Feng and B. T. Smith, Phys. Rev. D **71** (2005), 015004, K. Hamaguchi, M. Nojiri and A. de Roeck, J. High Energy Phys. **0703** (2007), 046.
- 16) M. Asplund, D. L. Lambert, P. E. Nissen, F. Primas and V. V. Smith, Astrophys. J. **644** (2006), 229, astro-ph/0510636.
- 17) E. Hiyama, Y. Kino and M. Kamimura, Prog. Part. Nucl. Phys. **51** (2003), 223.
- 18) C. Angulo *et al.*, Nucl. Phys. A **656** (1999), 3.

- 19) D. N. Spergel *et al.*, *Astrophys. J. Suppl.* **170** (2007), 377.
- 20) K. M. Nollett, R. B. Wiringa and R. Schiavilla, *Phys. Rev. C* **63** (2001), 024003.
- 21) M. Kamimura, *Phys. Rev. A* **38** (1988), 621.
- 22) M. Kamimura, *Muon Catal. Fusion* **3** (1988), 335.
- 23) Y. Kino and M. Kamimura, *Hyperfine Interact.* **82** (1993), 45.
- 24) K. Nagamine and M. Kamimura, *Adv. Nucl. Phys.* **24** (1998), 151.
- 25) M. Kamimura, *Prog. Theor. Phys. Suppl. No. 62* (1977), 236.
- 26) D.D. Clayton, *Principles of Stellar Evolution and Nuclear Synthesis* (The University of Chicago Press, 1983).
- 27) K. Ikeda, H. Horiuchi and S. Saito, *Prog. Theor. Phys. Suppl. No. 68* (1980), 1.
- 28) I. Tanihata *et al.*, *Phys. Rev. Lett.* **55** (1985), 2676.
- 29) S. Saito, *Prog. Theor. Phys.* **41** (1969), 705.
- 30) Y. Kino, N. Yamanaka, M. Kamimura, and H. Kudo, *Interactions* **146/147** (2003), 331.
- 31) W.-M. Yao *et al.* (Particle Data Group), *J. of Phys. G* **33** (2006), 1.
- 32) M. Hori *et al.*, *Phys. Rev. Lett.* **91** (2003), 123401.
- 33) M. Kawasaki, K. Kohri and T. Moroi, *Phys. Rev. D* **71** (2005), 083502.
- 34) I. Tanihata *et al.*, *Phys. Lett. B* **206** (1988), 592.
- 35) P. Descouvemont and D. Baye, *Nucl. Phys. A* **567** (1994), 341.
- 36) K. Varga, Y. Suzuki and I. Tanihata, *Phys. Rev. C* **52** (1995), 3013.
- 37) A. Cs ot o and K. Langanke, *Nucl. Phys. A* **636** (1998), 240.
- 38) H. Esbenson, *Phys. Rev. C* **70** (2004), 047603.
- 39) K. Ogata, S. Hashimoto, Y. Iseri, M. Kamimura and M. Yahiro, *Phys. Rev. C* **73** (2006), 024605.
- 40) M. Kamimura, *AIP Conf. Proc.* **181** (1989), 330.
- 41) J. Cohen, *Phys. Rev. A* **27** (1983), 167.
- 42) M. Kusakabe, private communication (2008).
- 43) K. Sumiyoshi, H. Utsunomiya, S. Goko and T. Kajino, *Nucl. Phys. A* **709** (2002), 467.
- 44) D. R. Tilley *et al.*, *Nucl. Phys. A* **745** (2004), 155.
- 45) K. Arai, P. Descouvemont, D. Baye and W. N. Catford, *Phys. Rev. C* **68** (2003), 014319; K. Arai, *Phys. Rev. C* **69** (2004), 014309; private communication (2008).
- 46) E. Hiyama, M. Kamimura, T. Motoba, T. Yamada and Y. Yamamoto, *Phys. Rev. C* **66** (2002), 024007; private communication on the radius of ^8Be .
- 47) E. Hiyama, M. Kamimura, T. Motoba, T. Yamada and Y. Yamamoto, *Prog. Theor. Phys.* **97** (1997), 881.
- 48) E. Hiyama, M. Kamimura, K. Miyazaki and T. Motoba, *Phys. Rev. C* **59** (1999), 2351.
- 49) E. Hiyama, M. Kamimura, T. Motoba, T. Yamada and Y. Yamamoto, *Phys. Rev. C* **65** (2001), 011301(R).